

Bond order from disorder in the planar pyrochlore magnet

O. Tchernyshyov*

Department of Physics and Astronomy, The Johns Hopkins University, Baltimore, Maryland, 21218

O. A. Starykh[†]

Department of Physics and Astronomy, Hofstra University, Hempstead, New York, 11549

R. Moessner[‡]

Laboratoire de Physique Théorique de l'École Normale Supérieure, CNRS-UMR8541, Paris, France

A. G. Abanov[§]

Department of Physics and Astronomy, Stony Brook University, Stony Brook, New York 11794-3800

(Dated: June 21, 2018)

We study magnetic order in the Heisenberg antiferromagnet on the checkerboard lattice, a two-dimensional version of the pyrochlore network with strong geometric frustration. By employing the semiclassical ($1/S$) expansion we find that quantum fluctuations of spins induce a long-range order that breaks the four-fold rotational symmetry of the lattice. The ordered phase is a valence-bond crystal. We discuss similarities and differences with the extreme quantum case $S = 1/2$ and find a useful phenomenology to describe the bond-ordered phases.

I. INTRODUCTION

Frustrated magnets have attracted the attention of theorists for several decades, beginning with the study of the Ising antiferromagnet on the triangular lattice.¹ More recently, new families of frustrated magnetic compounds have become available for experimental studies reviving the interest in their properties.^{2,3,4} By its very nature, a frustrated system has an extremely large classical degeneracy of the ground state. This degeneracy is very effective in suppressing classical spin order,⁵ thus providing a route to non-Néel (quantum) ground states even for higher-dimensional systems. The nature of such ground states is far from obvious: the aforementioned degeneracy allows for a variety of unusual vacua. Among the possibilities are bond-ordered states, in which pair averages $\langle \mathbf{S}_i \cdot \mathbf{S}_j \rangle$, rather than spins $\langle \mathbf{S}_i \rangle$ themselves, form a periodic pattern;^{6,7} and spin liquids that break no lattice symmetry but are distinguished by the unusual quantum numbers and statistics of their excitations.⁸

One of the most intensively studied frustrated systems is the Heisenberg antiferromagnet on the pyrochlore lattice. It has many experimental realizations that show rather remarkable magnetic behavior. For example, the spinel ZnCr_2O_4 is the first frustrated magnet in which zero modes—spin waves connecting degenerate ground states—have been observed by neutron scattering.⁹ Not long ago, it has been shown^{10,11} that a coupling between spins and lattice vibrations leads to a spin-Peierls phase transition in this manifestly three-dimensional spin system. This effect, also observed¹² in ZnCr_2O_4 , is classical in nature in the sense that it is not parametrically small in $1/S$. Therefore it is expected to dominate the more subtle quantum effects for large values of spin.

Effects of frustration in quantum pyrochlore antiferromagnets, particularly in the limit of a small spin S , are

drawing quite a bit of interest. Finding answers in this case may provide clues to the unusual behavior of underdoped cuprate superconductors, where frustration of the spin system is achieved through the motion of doped charges. Although replacing dynamic frustration with geometric one somewhat simplifies the problem, it is still far from trivial. An exact solution for $S = 1/2$ is not available and is not expected in the immediate future. Numerical diagonalizations are hampered by the quick growth of the Hilbert space with the lattice size in three dimensions. Several research groups are attacking the problem from various solvable limits: large S ,¹³ large N ,¹⁴ and weakly-coupled spin clusters.^{15,16,17,18,19} Because it is not even obvious that extrapolations from these limits will lead to a converging answer, it seems highly desirable to test these approaches on a similar problem for which numerical answers are available.

Most recently, a two-dimensional version of the pyrochlore network, the checkerboard lattice²⁰ (also known as the planar pyrochlore and the square lattice with crossings), has become a focus of analytical^{21,22,23} and numerical^{24,25,26,27} studies. Lower dimensionality of this system makes it an easier target for numerical approaches; at the same time, it has the local coordination of the pyrochlore lattice: magnetic bonds form a network of corner-sharing tetrahedra with spins at the vertices. It is therefore hoped that studies of the Heisenberg antiferromagnet on the checkerboard lattice can shed light on the behavior of its three-dimensional analog.

The planar pyrochlore lattice *does* differ from the pyrochlore proper in one fundamental aspect: not all bonds of its tetrahedra are equivalent—because no symmetry of the lattice turns first neighbors (horizontal and vertical bonds) into second (diagonal). Even if the corresponding exchange couplings J_1 and J_2 are set equal, spin correlations between first and second neighbors tend to be different, as evidenced by both analytical and numerical

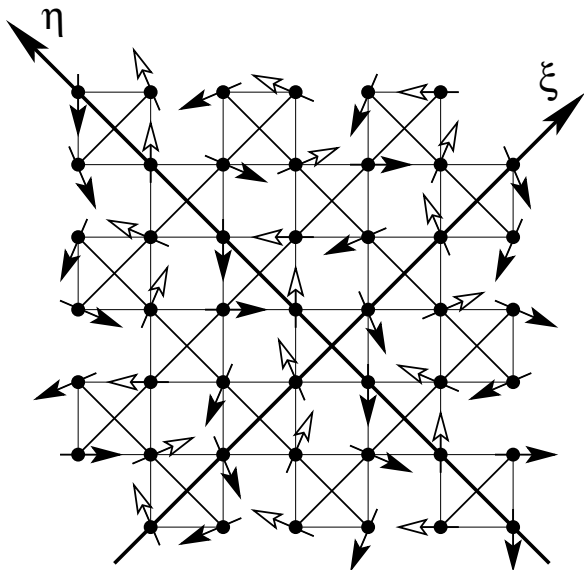


FIG. 1: Heisenberg antiferromagnet on the checkerboard lattice. Shown is a generic classical ground state for a model in which the second-neighbor coupling J_2 that exceeds the nearest-neighbor coupling J_1 . At the level of the classical approximation, the Néel order parameters of individual chains $\hat{\mathbf{n}}_i$ are uncorrelated. The direction $\hat{\mathbf{n}}_i$ is defined as that of spin \mathbf{S}_i at the left edge.

results. A lack of such symmetry compels one to look at the general case with $J_1 \neq J_2$.

In this work, we study the checkerboard antiferromagnet in the limit of large spin S , which allows for a systematic perturbation theory in powers of $1/S$.²⁸ We then compare our answers to the available numerical results for the opposite limit, $S = 1/2$, and find a simple phenomenology that describes both rather well. Our understanding of the checkerboard antiferromagnet has been greatly helped by three recent ideas: (a) Henley’s ‘gauge symmetry’ relating degenerate collinear ground states in a frustrated magnet;¹³ (b) casting of the problem in terms of bond—rather than spin—variables, which were introduced a decade ago by Harris *et al.*;⁶ (c) a realization of the potential significance of the $q = 3$ Potts model to bond-ordered states on the pyrochlore and checkerboard.

Because this paper is long and technical, the reader may find it helpful to peruse an informal introduction to the subject written by one of us.²⁹ That article states our reasons to pursue the large- S route to strongly frustrated quantum magnets, explains the challenges of that approach and points out ways to overcome them. It also contrasts the results obtained for different two-dimensional analogs of the pyrochlore lattice (the checkerboard is one of them).

The ground state of a classical ($S = \infty$) Heisenberg magnet is found by minimizing its energy

$$E_0 = \sum_{\langle ij \rangle} J_{ij} \mathbf{S}_i \cdot \mathbf{S}_j = \mathcal{O}(S^2) \quad (1)$$

with respect to classical spin variables \mathbf{S}_i . Exchange coupling is J_1 on horizontal and vertical bonds, and J_2 along diagonals. For weaker diagonal bonds, $J_2 < J_1$, classical energy minimization gives a unique ground state (modulo a global rotation of all spins). The ground state, shown in Fig. 2(a), is the same as that of the simple square lattice ($J_2 = 0$).

In the region $J_2 \geq J_1$, the classical ground state becomes continuously degenerate. For stronger diagonal bonds, $J_2 > J_1$, the system can be viewed as a collection of criss-crossing chains running along diagonals of the lattice (Fig. 1). Let us choose north-east to be our positive $\hat{\xi}$ -direction, and north-west to be $\hat{\eta}$. Classically, each chain has perfect Néel order at zero temperature, however, directions of staggered magnetizations $\hat{\mathbf{n}}_i$ of different chains are completely independent at the classical level. In an $L \times L$ lattice with periodic boundary conditions classical ground states can be parametrized by L unit vectors $\hat{\mathbf{n}}_i$. The classical degeneracy increases even further in the case of equal exchanges $J_2 = J_1$.^{30,31}

The first-order (in $1/S$) correction to the classical energy comes from the zero-point quantum fluctuations of spin waves,

$$E_1 = \sum_k \hbar |\omega_k| / 2 = \mathcal{O}(S), \quad (2)$$

where $\{\omega_k\}$ are eigenfrequencies of classical spin waves about a given ground state obtained from the equations of motion

$$\hbar \dot{\mathbf{S}}_i = \sum_j J_{ij} \mathbf{S}_i \times \mathbf{S}_j. \quad (3)$$

It has been established previously that, quite generally, quantum fluctuations select ground states with collinear spins (assuming such classical ground states exist).^{32,33}

For a fixed global direction $\hat{\mathbf{n}}$, the problem thus reduces to a minimization of the zero-point energy (2) over a discrete set of collinear Néel states. Thus selected ground states can be characterized in the thermodynamic limit with the aid of some order parameters. In addition to violating the spin-rotation symmetry $O(3)$, these ground states can also break some discrete lattice symmetries. For instance, when the ground states are not symmetric under $\pi/2$ rotations of the plane, one expects an order parameter with the structure $\mathbf{Z}_2 \times \mathbf{S}^2$. For a given direction of the Néel vector, there should then be *two* degenerate ground states. (See, e.g., the work by Chandra *et al.*³⁴ on the square lattice with a large second-neighbor coupling.) Contrary to these expectations, we find that for $J_2 > J_1$ the ground state is *fourfold* degenerate with an order parameter $\mathbf{Z}_2 \times \mathbf{Z}_2 \times \mathbf{S}^2$. The extra degeneracy turns out to be related to a gauge-like symmetry (due to Henley¹³) that exists at the order $1/S$ in the semiclassical expansion. This dynamical symmetry is responsible for an even higher degeneracy of the ground state at the most frustrated point $J_1 = J_2$. In that case, the Néel order is destroyed and the order parameter is reduced

to $\mathbf{Z}_2 \times \mathbf{Z}_2 \times \mathbf{S}^2/\mathbf{Z}_2$ (two Ising orders and a director). At $J_1 = J_2$ the planar pyrochlore is a valence-bond solid with two independent bond orders and a nematic spin order.

The paper is organized in the following way. In most of it (Sections II through V) we study the lowest-order— $\mathcal{O}(1/S)$ —quantum corrections to the degenerate classical limit. We first explore the case where the second-neighbor coupling J_2 dominates and the system can be viewed as a set of weakly coupled antiferromagnetic chains. The interchain coupling J_1 is frustrated and has no effect at the classical level. We show in Sec. II that, in line with the standard arguments,^{32,33} quantum fluctuations favor collinear spin states. By using J_1/J_2 as a small parameter, we derive an effective interaction between the chains generated by quantum fluctuations. This potential is minimized by *four* distinct classical states. In Sec. III we prove that this degeneracy remains intact for all $J_1 < J_2$ and trace its origins to Henny’s gauge symmetry. Sec. IV presents our findings in the strongly frustrated case of equal exchange couplings. This time, a much larger degeneracy of the ground state kills the Néel order (replacing it with a nematic order), but the bond order survives. A summary of the large- S results is given in Sec. V. Finally, in Sec. VI we explore the connection of these large- S results to the $S = 1/2$ phase diagram obtained in numerical studies and speculate on a phenomenology of the bond order in the $S = 1/2$ case.

II. WEAKLY COUPLED CHAINS: $J_1 \ll J_2$

For $J_1 = 0$, the magnet is reduced to a collection of independent antiferromagnetic chains running along the diagonals (Fig. 1). In a classical ground state, each chain has perfect antiferromagnetic order. For this reason, there is no coupling between intersecting chains at the classical level—even in the presence of a finite interchain coupling $J_1 < J_2$.

Quantum fluctuations disrupt the perfect Néel alignment of adjacent spins and thus enable the chains to interact. For a weak interchain coupling $J_1 \ll J_2$, one can use a systematic perturbation theory in J_1/J_2 (staying at the same order in $1/S$) developed by Shender.³⁵

A. Effective interactions between chains

To the lowest nontrivial order in J_1/J_2 , the interchain coupling generates a potential that selects collinear spin configurations. For Néel magnetizations of individual chains $\hat{\mathbf{n}}_m$,

$$E^{(2)} = -\frac{4 - \pi}{2\pi} \frac{J_1^2 S}{J_2} \sum_{\text{crossings}} (\hat{\mathbf{n}}_m \cdot \hat{\mathbf{n}}_n)^2. \quad (4)$$

This interaction—coupling any two chains intersecting over a tetrahedron—is minimized when all staggered

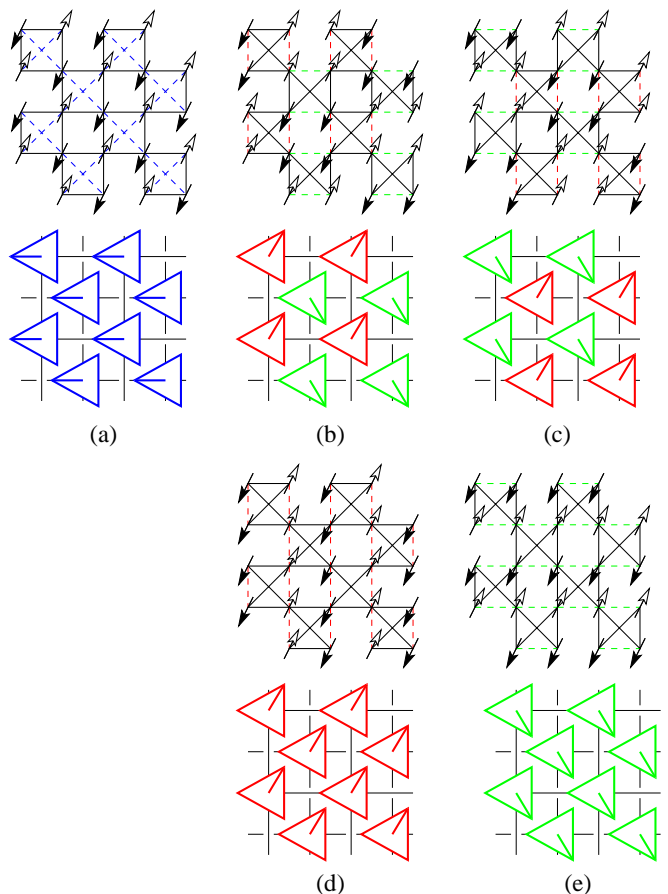


FIG. 2: (a) The classical ground state for $J_1 > J_2$. (b) through (e) are the four classical ground states at the order $1/S$ for $J_1 \leq J_2$. Frustrated bonds (those with two parallel spins) are shown in color dashed lines. Bottom figures show the lattice of tetrahedra; the primary colors (red, green, and blue) encode the location of frustrated bonds. See Fig. 3 for more details.

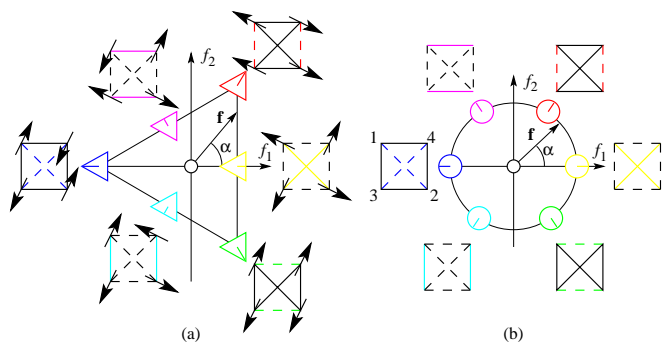


FIG. 3: Bond variables $\mathbf{f} = (f_1, f_2)$ for a single tetrahedron in a ground state $\sum_{i=1}^4 \mathbf{S}_i = 0$. See Eq. (20) for a definition of \mathbf{f} . (a) Classical $S = 1/2$. In both cases, primary colors denote the pure states with two frustrated bonds (parallel classical spins or a spin triplet). Secondary colors mark the pure states with two satisfied bonds (antiparallel spins or a spin singlet). The triangle and the circle delineate the domains of attainable values.

magnetizations point along a common axis, $\hat{\mathbf{n}}_m = \pm \hat{\mathbf{n}}$. The tendency of spins to align is the standard outcome of the order-from-disorder scenario.^{32,33} See Appendix for a derivation of Eq. (4).

Collinear Néel states can be characterized by a collection of Ising variables: $s_m = \pm 1$ for chains running along the direction $\hat{\xi}$ and $t_m = \pm 1$ for chains along $\hat{\eta}$, see Fig. 1. Given a global orientation of spins $\hat{\mathbf{n}}$, these numbers determine the staggered magnetizations of individual chains, $\hat{\mathbf{n}}_m = s_m \hat{\mathbf{n}}$ or $t_m \hat{\mathbf{n}}$, respectively. To the fourth order in J_1 (but still to the first order in $1/S$) we obtain the correction to the classical energy of the ground state

$$E^{(4)} = \frac{2J_1^4 S}{J_2^3} \sum_{k=1}^{\infty} \sum_{l=1}^{\infty} \sum_m \sum_n (A_{2k} s_m s_{m+2k} + A_{2l} t_m t_{m+2l} - B_{2k-1, 2l-1} s_m s_{m+2k-1} t_n t_{n+2l-1}), \quad (5)$$

where the positive coefficients A_l and B_{kl} are computed in the Appendix. Note that there is no pairwise interaction between adjacent parallel chains (nor, for that matter, between any parallel chains an odd distance apart). As a result of that, the effective interaction (5) is invariant under the transformation

$$s_m \mapsto (-1)^m s_m, \quad t_n \mapsto (-1)^n t_n, \quad (6)$$

which flips the spins on every other diagonal chain.

B. Ground states

The largest term in Eq. (5) is the interaction of 4 chains intersecting around an empty plaquette:

$$- \frac{2J_1^4 S}{J_2^3} \sum_m \sum_n B_{1,1} s_m s_{m+1} t_n t_{n+1} \quad (7)$$

(see Appendix for details). It is minimized by ground states of two distinct kinds:

$$s_m = s_{m+1}, \quad t_n = t_{n+1}, \quad \text{Fig 2(b) and (c),} \quad (8)$$

$$s_m = -s_{m+1}, \quad t_n = -t_{n+1}, \quad \text{Fig 2(d) and (e).} \quad (9)$$

Curiously, the two types of ground states (8) and (9) are related to each other by the staggering transformation (6), rather than by any symmetry of the lattice. They remain degenerate even upon the inclusion of all two- and four-chain interactions in Eq. (5). The origin of this dynamical symmetry will be discussed in Sec. III.

C. Long-range spin order

It is natural to ask whether there is a long-range spin order in the system. Quantum effects turn out to be rather subtle in this case. On the one hand, quantum fluctuations tend to destroy the long-range order found

on classical chains. On the other, they create interchain coupling and make the system two-dimensional thereby making spin order more likely. Which tendency wins?

To answer this question one can compute the expectation values of local magnetization $\langle \mathbf{S}_r \rangle$ in one of the ground states [Fig. 2(b) through (e)]. The classical value $(0, 0, \pm S)$ is reduced by quantum fluctuations of spins. A naïve evaluation of this quantity at the first order in $1/S$ gives a divergent negative correction suggesting that the order is destroyed. This, however, is an artefact of a low-order approximation. The magnon spectrum is given by the frequencies of *classical* spin waves, which know nothing about the interchain coupling. As a result, the magnon spectrum contains *lines* of zero modes along the diagonal directions ($p_\xi = 0, \pi$ and $p_\eta = 0, \pi$). The abundance of soft modes leads to a destruction of the long-range spin order.

At the next level of approximation, $\mathcal{O}(1/S^2)$, magnon interactions modify the spin-wave spectrum lifting the zero modes to finite frequencies (with the exception of isolated points in the Brillouin zone).³⁶ The spin excitations become two-dimensional and the infrared divergence of the correction to local magnetization is removed. Long-range order can survive.

Alternatively, the hardening of the spin-wave spectrum (specifically of the zero modes) can be evaluated already at the order $\mathcal{O}(1/S)$ by adding to the Heisenberg Hamiltonian a phenomenological biquadratic exchange term^{33,37}

$$V_{\text{bi}} = -K \sum_{\mathbf{r}, \mathbf{r}'} (\mathbf{S}_r \cdot \mathbf{S}_{r'})^2 \quad (10)$$

that couples spins at the intersections of chains. The strength of this interaction $K = \mathcal{O}(J_1^2/J_2 S^3)$ is chosen so as to mimic, at the classical level, the energy of zero-point fluctuations. The latter is given, to the lowest order in J_1 , by Eq. (A.24). The spin-wave spectrum is then computed from the classical equations of motion for the spins.

By performing a calculation along these lines (to be reported elsewhere³⁸) we find that indeed the zero modes acquire energies of order $J_1 \sqrt{S}$. The renormalized magnon frequency vanishes at the points

$$(p_\xi, p_\eta) = (0, 0) \text{ and } (\pi, \pi) \quad (11)$$

only, as required by the Goldstone theorem. The average local magnetization reads

$$\langle S^z \rangle = S - 2 \ln \frac{J_2 \sqrt{S}}{J_1} + \text{regular terms.} \quad (12)$$

The correction to the classical value S is a remnant of the logarithmic divergence in one dimension that has been regularized by an infrared cutoff $\omega_{\text{min}} = \mathcal{O}(J_1 \sqrt{S})$ brought about by the interchain coupling (10). The argument of the logarithm is the ratio of the maximum magnon frequency $\omega_{\text{max}} = \mathcal{O}(J_2 S)$ to the infrared cutoff.

Taking this formula at face value we estimate that the Néel order is present if the interchain exchange exceeds a critical value

$$J_{1c} = \mathcal{O}(J_2 \sqrt{S} e^{-S/2}). \quad (13)$$

Note that the ordering is a truly collective effect since independent spin chains possess no LRO. This feature makes the order-by-disorder problem rather different from its higher-dimensional analogues where each individual unit (say, spin plane in a canonical example of two interpenetrating square lattices) is ordered even in the absence of frustrating inter-unit interactions. Finally, Eq. (13) indicates that at a large S there is a narrow region of ratios J_1/J_2 without Néel order. This result is in agreement with a weak-coupling renormalization group analysis of the $S = 1/2$ problem by one of us¹⁹ who argued in favor of a gapless sliding Luttinger liquid ground state in a wide interval $0 \leq J_1/J_2 \leq 0.8$.

III. CROSSED CHAINS: $J_1 < J_2$

The four vacua [Fig. 2(b)–(e)] found in the limit of weakly coupled chains, $J_1 \ll J_2$, remain the ground states of the system for all finite ratios $J_1/J_2 < 1$. To confirm this, we have computed numerically spin-wave spectra of all collinear classical ground states for a lattice 16×16 with periodic boundary conditions. Modulo the global $O(3)$ spin symmetry, there are $2^{16} = 65536$ spin configurations to consider. The energy of zero-point motion (2) is indeed minimized by the four Néel states (8–9). In fact, not only they remain degenerate (with numerical accuracy): their spin-wave spectra are identical. That surely means that there is a hidden symmetry at work.

The observed fourfold degeneracy is caused by a special gauge-like symmetry discovered by Henley.¹³ It exists whenever a lattice can be split into corner-sharing units (tetrahedra on the pyrochlore lattice, second-neighbor pairs in the present case) with total zero spin in any ground state. *Nonzero* eigenfrequencies of such a system can be obtained by solving the equations of motions for the transverse components of the total spins of these units $(\text{Re}\sigma_\alpha, \text{Im}\sigma_\beta)$, which have the following simple form:^{30,31}

$$i \dot{\sigma}_\alpha = \sum_{\beta \neq \alpha} J_{\alpha\beta} S_{\alpha\beta} \sigma_\beta. \quad (14)$$

Here $S_{\alpha\beta}$ is the ordered (longitudinal) component of the spin shared by units α and β . It can now be seen that whenever two ground states are related by an Ising gauge transformation

$$S'_{\alpha\beta} = \Lambda_\alpha S_{\alpha\beta} \Lambda_\beta^{-1}, \quad \Lambda_\alpha = \pm 1, \quad (15)$$

their nonzero modes are also related,

$$\sigma'_\alpha = \Lambda_\alpha \sigma_\alpha, \quad (16)$$

and have identical frequency spectra. Therefore gauge-equivalent ground states have the same zero-point energy.

In the current context, sites α of the dual lattice are “tetrahedra” (squares with crossings) of the original checkerboard lattice. For equal exchanges $J_2 = J_1$, a unit contains four spins whose total spin vanishes in a ground state. For strong diagonal chains ($J_2 > J_1$), the total spin must vanish on both diagonal bonds separately, so that there are two units on every site of the dual lattice: the diagonal links ξ and η . The resulting equations for a collinear Néel state read

$$\begin{aligned} i\dot{\mu}_{\mathbf{r}} &= S_{\mathbf{r},\mathbf{r}+\hat{\xi}}(J_2\mu_{\mathbf{r}+\hat{\xi}} + J_1\nu_{\mathbf{r}+\hat{\xi}}) \\ &+ S_{\mathbf{r},\mathbf{r}-\hat{\xi}}(J_2\mu_{\mathbf{r}-\hat{\xi}} + J_1\nu_{\mathbf{r}-\hat{\xi}}) \\ i\dot{\nu}_{\mathbf{r}} &= S_{\mathbf{r},\mathbf{r}+\hat{\eta}}(J_1\mu_{\mathbf{r}+\hat{\eta}} + J_2\nu_{\mathbf{r}+\hat{\eta}}) \\ &+ S_{\mathbf{r},\mathbf{r}-\hat{\eta}}(J_1\mu_{\mathbf{r}-\hat{\eta}} + J_2\nu_{\mathbf{r}-\hat{\eta}}), \end{aligned} \quad (17)$$

where \mathbf{r} are coordinates of a tetrahedron. A spin labelled $\mathbf{S}_{\mathbf{r}\mathbf{r}'}$ is shared by the tetrahedra located at \mathbf{r} and \mathbf{r}' . Finally, $\mu_{\mathbf{r}}$ and $\nu_{\mathbf{r}}$ are transverse spin components of its units:

$$\begin{aligned} \mathbf{S}_{m-\frac{1}{2},n} + \mathbf{S}_{m+\frac{1}{2},n} &= (\text{Re}\mu_{mn}, \text{Im}\mu_{mn}, 0), \\ \mathbf{S}_{m,n-\frac{1}{2}} + \mathbf{S}_{m,n+\frac{1}{2}} &= (\text{Re}\nu_{mn}, \text{Im}\nu_{mn}, 0) \end{aligned} \quad (18)$$

in the notations of Fig. 1.

The transformation (15–16) does not actually reflect a local symmetry: applied to a single unit, α , it flips the spins $S_{\alpha\beta}$ shared by α with other units β . These other units acquire a nonzero total spin and violate the ground-state condition. Therefore the transformations must be made on a number of dual sites (an infinite one for an infinite lattice). For $J_2 > J_1$, entire diagonal chains of spins must be flipped. It can be checked that the two ground states shown in Fig. 2 (b) and (d) are related through such a gauge transformation flipping spins on every other diagonal chain in both directions.

In addition to breaking the spin $O(3)$ symmetry, the 4 ground states also violate the spatial symmetry of the checkerboard lattice. This leads to interesting consequences. Although the spin symmetry must be restored at any finite temperature (the Mermin–Wagner theorem), the discrete lattice symmetries need not. In such a case, the low-temperature phase can have a long-range spin-Peierls (bond) order. An example of such behavior was discovered by Chandra *et al.*³⁴ for the Heisenberg antiferromagnet on the square lattice with large second-neighbor coupling.

To see the pattern of bond order in the proposed spin-Peierls states one can look at the bond averages $\langle \mathbf{S}_i \cdot \mathbf{S}_j \rangle$ in the ground states of Fig. 2 (b)–(e). We have shown the frustrated bonds (those with parallel spins) in color depending on the bond orientation: red for vertical and green for horizontal ones. The lower part shows the dual lattice of “tetrahedra” each painted in the corresponding color. Using this language, the ground states can be described in a simple manner: *second* neighbors on the dual lattice have the same color. In fact, if the dual

sublattice is divided into two sublattices, each sublattice exhibits “ferromagnetic” Ising order—in terms of these color variables—independently of the other sublattice. Hence a fourfold degeneracy mentioned above.

An ordered state thus can be completely characterized by a composite order parameter $\mathbf{Z}_2 \times \mathbf{Z}_2 \times \mathbf{S}_2$: two independent Ising variables and a Néel vector. The Ising order parameter,

$$f_2 = \langle (\mathbf{S}_{\mathbf{r},\mathbf{r}+\hat{\xi}} - \mathbf{S}_{\mathbf{r},\mathbf{r}-\hat{\xi}}) \cdot (\mathbf{S}_{\mathbf{r},\mathbf{r}+\hat{\eta}} - \mathbf{S}_{\mathbf{r},\mathbf{r}-\hat{\eta}}) \rangle, \quad (19)$$

has a counterpart in the frustrated antiferromagnet on the square lattice with a second-neighbor coupling.³⁴ However, we will find a richer structure of ground states because our order parameter is, in fact, a component of a doublet $\mathbf{f} = (f_1, f_2)$, defined for every tetrahedron:

$$\begin{aligned} f_1 &= \frac{\langle (\mathbf{S}_1 + \mathbf{S}_2) \cdot (\mathbf{S}_3 + \mathbf{S}_4) - 2(\mathbf{S}_1 \cdot \mathbf{S}_2 + \mathbf{S}_3 \cdot \mathbf{S}_4) \rangle}{\sqrt{12}}, \\ f_2 &= \frac{\langle (\mathbf{S}_1 - \mathbf{S}_2) \cdot (\mathbf{S}_3 - \mathbf{S}_4) \rangle}{2}. \end{aligned} \quad (20)$$

[Fig. 3(a)]. The other component, f_1 , comes into play when the vertical and horizontal bonds become (nearly) equivalent to the diagonal ones, a situation encountered on the three-dimensional pyrochlore lattice.¹¹

IV. PLANAR PYROCHLORE: $J_1 = J_2$

This is a point with a very large *classical* degeneracy.^{30,31} Only the total spin of a “tetrahedron” must vanish in a ground state, but not necessarily the spins of second-neighbor pairs separately. To the next order, $\mathcal{O}(1/S)$, numerical comparison of zero-point fluctuation energies in collinear Néel states still reveals a large degeneracy—much larger than in the previously discussed case $J_2 > J_1$. The ground states of Fig. 2 (b)–(e) become degenerate with the Néel state of the simple square lattice [Fig. 2(a)] and many others numbering 2^L in total. Apparently this multitude of degenerate ground states kills the long-range Néel order. On the other hand, it will be seen that the bond order survives.

To proceed, we present an explicit construction of all collinear ground states degenerate at the $1/S$ level, and identify a short-range interaction that selects these ground states. It turns out that the most economical description of these states is obtained in terms of the bond—rather than spin—variables.

A. Gauge-equivalent collinear states

For equal exchanges, Eq. (14) holds for quartets of spins on “tetrahedra” of the checkerboard lattice (squares with crossings). As far as collinear Néel states are concerned, there are now three distinct possibilities: parallel spins can be found on vertical, horizontal, and now also diagonal bonds, which we encode, respectively, as red,

green, and blue states of a tetrahedron. In the Néel state of the simple square lattice [Fig. 2(a)] all diagonal bonds have parallel spins, so that this state is uniformly blue. After casting Henley’s gauge principle in bond language, we will readily reproduce all collinear Néel states degenerate with the blue vacuum. The four ground states found in the $J_2 > J_1$ case [Fig. 2 (b)–(e)] are among these.

As before, a gauge transformation on a tetrahedron involves flipping all its spins. Parallel spins are found on the same bonds before and after the transformation, therefore the color of that tetrahedron remains unchanged; it is the colors of its neighbors that are affected. Therefore, gauge transformations can be done *separately and independently* on the two sublattices of tetrahedra.

Flipping the four spins $S_{\alpha\beta}$ on tetrahedron α from sublattice A takes four adjacent tetrahedra $\beta \in B$ out of the ground state. To fix this problem, for each β we must perform at least one more gauge transformation on one of *its* neighbors $\gamma \in A$. Here are the rules for gauge transformations performed on sublattice A:

- (a) For every tetrahedron $\beta \in B$, the number of gauge transformations $\Lambda_\alpha = -1$ on adjacent tetrahedra $\alpha \in A$ can be 0, 2, or 4.
- (b) If this number is 0 or 4, β remains blue.
- (c) For 2 gauge transformations, the two α *cannot* be on opposite sides of β (e.g., northeast and southwest).
- (d) If both α are north of β (or both are south of β), β becomes red. If both α are east (west) of β , it turns green.

By using these rules, we can now construct an arbitrary ground state starting with the blue one. As the ground state is a direct product of independent ground states on sublattices A and B, we will construct a ground state of sublattice B by making gauge transformations on sublattice A. Suppose, for definiteness, that there is a red tetrahedron on sublattice B and that the two gauge transformations were made north of it [Fig. 4(a)]. If no other gauge transformations were made, this state would violate Rule (a): the two B tetrahedra shown in black are not in their ground states. Additional gauge transformations cannot be made around the original red site, for it will become blue [Fig. 4(b)], contrary to the initial assumption. The only remaining possibility is shown in Fig. 4(c): additional gauge transformations are made on the same horizontal line. Continuing the process we find a line of red tetrahedra extending over the entire sublattice B in the horizontal direction [Fig. 4(d)]. Thus a generic ground state of one sublattice consists of horizontal red and blue stripes of arbitrary widths [Fig. 4(e,f)] or of vertical green and blue stripes [Fig. 4(g)].

The process is then repeated with the roles of the sublattices reversed: sublattice A is colored via gauge transformations on sublattice B (whose colors are unchanged). A sample ground state is shown in Fig. 4(h).

Now it is easy to count the number of degenerate ground states on an $L \times L$ checkerboard lattice with periodic boundary conditions. On a single sublattice of tetrahedra, there are $2 \times 2^{L/2-1}$ red-and-blue ground states: the exponential reflects the number of ways to place horizontal domain walls separating red and blue stripes; the prefactor accounts for a duplicate set of states with red and blue domains exchanged. In addition, there is an equal number of green-and-blue states bringing the total to $2^{L/2+1} - 1$ per sublattice. (The blue state has been counted twice.) The total degeneracy of the ground state (including both sublattices of tetrahedra) is therefore of order 2^L .

B. Long-range bond order

Is there a spontaneously broken symmetry? There's definitely no long-range *vector* order. It is easy to see that two spins located on the same diagonal can be parallel and antiparallel with an equal probability: they are parallel if there is an even number of nonblue tetrahedra in between, antiparallel if the number is odd. By construction (Fig. 4), the probabilities of these outcomes are equal and $\langle \mathbf{S}_r \cdot \mathbf{S}_{r'} \rangle = 0$ for these two spins: there is not even a short-range order. The argument can be extended to (almost) any other direction. (Exceptions are the vertical and horizontal directions: there are long-range correlations of spins along the horizontal or vertical lines of bonds in the cyan and magenta states.)

The only remnant of the spin order is the collinearity of spins: $(\mathbf{S}_r \cdot \mathbf{S}_{r'})^2 = S^4$ in any ground state for any pair of spins. Thus one can conclude that the ground state is a spin nematic whose order parameter is a *director* (S^2/Z_2).

In addition, the system has long-range *bond* order. Indeed, if one tetrahedron on sublattice A is colored red, there are no green tetrahedra anywhere on the same sublattice—and vice versa. Thus the symmetry between red and green colors (the symmetry between vertical and horizontal bonds) is spontaneously broken. The average color of a given tetrahedron is magenta (red and blue stripes) or cyan (green and blue). Each sublattice finds itself in the cyan or magenta phase, Figs. 4(i,j). In the cyan phase, the vertical (“red”) bonds feature antiparallel spins; in the magenta phase, antiparallel spins are found on horizontal (“green”) bonds. The colors of the sublattices are *independent* at order $1/S$.

This argument can be made more precise by turning to the bond order parameter f_2 (20). As shown in Fig. 3(a), f_2 is positive, zero, and negative in the red, blue, and green states, respectively. Averaging over the entire ground state manifold gives $\langle f_2(\mathbf{r}) \rangle = 0$ for any tetrahedron. The reasoning put forward in the previous paragraph suggests that $\langle f_2(\mathbf{r})f_2(\mathbf{r}') \rangle = S^4/2 > 0$ even as $|\mathbf{r} - \mathbf{r}'| \rightarrow \infty$ (as long as the tetrahedra \mathbf{r} and \mathbf{r}' reside on the same sublattice). Thus a long-range bond order is present.³⁹

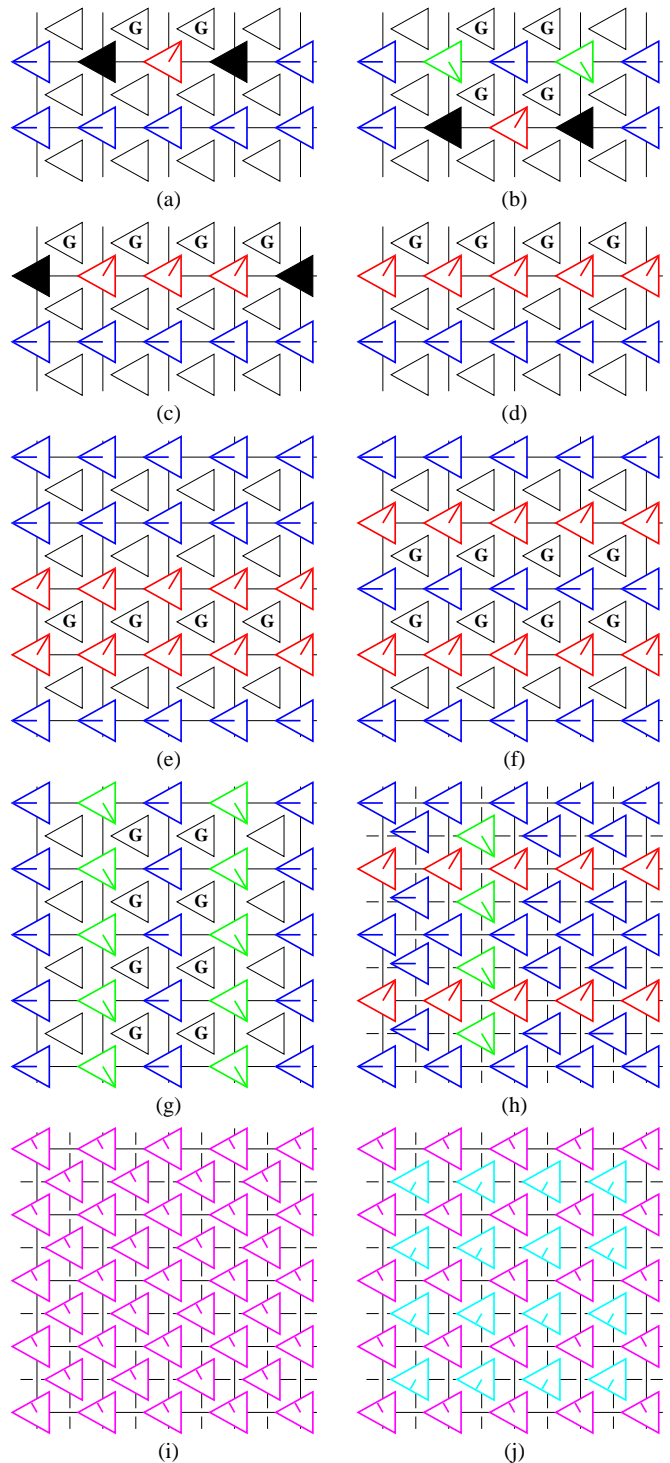


FIG. 4: Construction of ground states at the order $1/S$ for $J_1 = J_2$. The secondary color magenta is an equal-part mixture of red and blue; similarly, cyan is an equally-weighted average of green and blue. The letter G marks the locations of Z_2 gauge transformations. Filled triangles represent tetrahedra not in a ground state.

The long-range order is thus similar to the case $J_1 < J_2$, with one exception: the Néel vector in the composite order parameter is replaced with a director that defines a collinearity axis. The order parameter now has the structure $\mathbf{Z}_2 \times \mathbf{Z}_2 \times \mathbf{S}^2/\mathbf{Z}_2$: two Ising order parameters in addition to a spin nematic. The spin-nematic order breaks a continuous rotational symmetry and therefore will be lost at any finite temperature. The remaining Ising orders $\mathbf{Z}_2 \times \mathbf{Z}_2$ are expected to survive up to a finite temperature $\mathcal{O}(JS)$.

C. Effective spin interaction

One may wonder what kind of a Hamiltonian gives rise to a strongly degenerate set of ground states described above. In fact, it can be derived following Henley's method.¹³ The quantum correction of order $1/S$ to the ground state energy (2) is obtained by rewriting Eq. (14) for the eigenmodes:

$$\begin{aligned} \hbar^2 \omega^2 \sigma_\alpha &= J^2 \sum_{\beta(\alpha)} \sum_{\gamma(\beta)} S_{\alpha\beta} S_{\beta\gamma} \sigma_\gamma \\ &= 4J^2 S^2 \sigma_\alpha + J^2 \sum_{\beta(\alpha)} \sum_{\gamma(\beta) \neq \alpha} S_{\alpha\beta} S_{\beta\gamma} \sigma_\gamma. \end{aligned} \quad (21)$$

The notation $\beta(\alpha)$ indicates that tetrahedron β is a neighbor of tetrahedron α (they share spin $S_{\alpha\beta}$). Following Henley, we introduce an adjacency matrix,

$$T_{\alpha\gamma} = -\frac{1}{2S^2} \sum_{\beta(\alpha,\gamma)} S_{\alpha\beta} S_{\beta\gamma}, \quad (22)$$

whose matrix elements are nonzero when tetrahedra α and γ have a common neighbor β . The sum over nonzero eigenfrequencies can now be expressed in terms of the matrix T :

$$\sum_n \frac{\hbar|\omega_n|}{2} = JS \text{Tr} \sqrt{1-T} = JS \text{Tr} \left(1 - \frac{T}{2} - \frac{T^2}{8} - \dots \right). \quad (23)$$

This expansion converges rather slowly (eigenvalues of T extend all the way up to 1) and cannot be used for quantitative purposes. Nevertheless, it provides correct qualitative answers, as will be seen shortly.

Because $T_{\alpha\alpha} = 0$, the first spin-dependent correction comes from the second-order term,

$$-\frac{JS}{4} \text{Tr} T^2 = -3JSL^2 - \frac{J}{4S^3} \sum_{\alpha\beta\gamma\delta} S_{\alpha\beta} S_{\beta\gamma} S_{\gamma\delta} S_{\delta\alpha}. \quad (24)$$

(In the last sum, all tetrahedra are distinct.) This spin-dependent term can be considered as a four-body interaction of spins or as a two-body interaction of bond variables. Indeed, the interaction $-S_{\alpha\beta} S_{\beta\gamma} S_{\gamma\delta} S_{\delta\alpha}$ is minimized when the number of down spins is even, which can be cast in bond language as

$$S_{\alpha\beta} S_{\beta\gamma} = S_{\gamma\delta} S_{\delta\alpha} = \pm S^2, \quad (25)$$

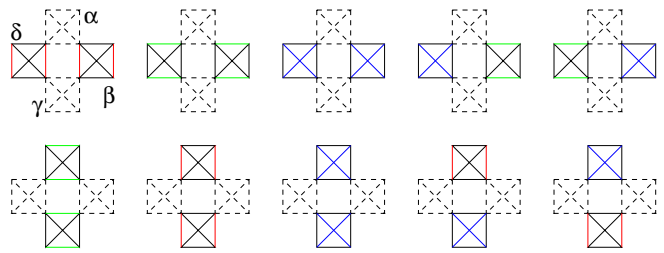


FIG. 5: Ground states of Henley's four-spin interaction, Eq. (24). Frustrated bonds are shown in color. Parametrization in terms of bond (rather than spin) variables decouples tetrahedra of one sublattice (α, γ) from those of the other (β, δ).

i.e., when the *vertical* bonds of tetrahedra β and δ simultaneously have parallel or antiparallel spins. All such bond configurations are shown in the top row of Fig. 5. Alternatively, this 4-spin term can be considered as a bond interaction between tetrahedra α and γ , which is minimized when

$$S_{\delta\alpha} S_{\alpha\beta} = S_{\beta\gamma} S_{\gamma\delta} = \pm S^2, \quad (26)$$

i.e., when their *horizontal* bonds simultaneously have parallel or antiparallel spins. These ground states are shown in the bottom part of Fig. 5.

Note that the bond interaction generated by the term $-\text{Tr} T^2$ is between tetrahedra of the same sublattice. Higher-order spin loops $-\text{Tr} T^n$ can also be represented as an interaction between n tetrahedra of the same sublattice. In terms of bond variables, there is no coupling between different sublattices at the order $1/S$.

Before deriving the three-body interaction, it makes sense to check for the ground states of the two-body bond Hamiltonian that we have just obtained: the energy is -1 for states shown in Fig. 5 and $+1$ for the remaining states. More concisely,

For tetrahedra on the same sublattice, nearest neighbors in the horizontal direction need to be both red or neither red; in the vertical direction both green or neither green.

It is easy to see that this rule gives precisely all the ground states found in the beginning of this Section by means of Henley's gauge argument—and no other states.

It is quite remarkable that a crude two-body approximation,

$$\text{Tr} \sqrt{1-T} \approx \text{Tr} (1 - T/2 - T^2/8), \quad (27)$$

correctly reproduces all the ground states. This fact seems to indicate that the neglected n -body interactions (which are by no means small) can be expressed in terms of the two-body potentials identified above. If this is the case, the many-body interactions shift all ground states by the same amount without breaking their degeneracy. (We have checked that the 3 and 4-body interactions are indeed reducible.)

D. Effective bond interaction

The four-spin interaction (24) can also be written in terms of the bond variables (20). Adjacent tetrahedra α and γ of the same sublattice (Fig. 5) interact with energy

$$E_{\alpha\gamma} = -\frac{JS}{8} \left(\frac{1}{3} + \frac{\mathbf{f}_\alpha \cdot \hat{\mathbf{n}}_{\alpha\gamma}}{S^2\sqrt{3}} \right) \left(\frac{1}{3} + \frac{\mathbf{f}_\gamma \cdot \hat{\mathbf{n}}_{\alpha\gamma}}{S^2\sqrt{3}} \right). \quad (28)$$

The unit vector $\hat{\mathbf{n}}_{\alpha\gamma}$ points in the red direction [Fig. 3(a)] for neighbors along $\hat{\mathbf{x}}$ and in the green direction for neighbors along $\hat{\mathbf{y}}$. The one-body piece can be viewed as a “magnetic” field for the two-component “spin” \mathbf{f}_α that points in the cyan or magenta direction. Once we sum over all neighbors of a given tetrahedron, the resulting “magnetic field” has the blue color and the magnitude $J/4S^3\sqrt{3}$. The two-body potential couples ferromagnetically the red or green components of neighboring “spins” depending on the direction.

It is worth noting that a very similar interaction has been obtained for the quantum case $S = 1/2$ by Tsunetsugu.^{16,17} We will return to this point later in Sec. VI.

V. LARGE S : A BRIEF SUMMARY

Our study of the ground state of the Heisenberg checkerboard antiferromagnet to order $1/S$ establishes the existence of a long-range bond order in this system. The bond order breaks a mirror symmetry of the lattice exchanging the vertical and horizontal directions (the green and red colors in our notation). The discrete (\mathbf{Z}_2) nature of the broken symmetry assures survival of the long-range bond order to finite temperatures. It is instructive to trace the evolution of the ground state as the ratio of the first and second-neighbor exchange couplings varies.

For $J_2/J_1 < 1$, the ground state is unique (up to a global rotation of all spins): it is the Néel state of the simple square lattice ($J_2 = 0$). Although the global $O(3)$ spin symmetry is broken at $T = 0$, it is restored at any finite temperature. The \mathbf{Z}_2 symmetry is manifest.

For $J_2/J_1 > 1$, we find a fourfold degeneracy as each sublattice independently chooses one of the two ground states with collinear spins. In the red state, *parallel* spins are found on vertical bonds (and antiparallel spins on all other bonds). In the green state, parallel spins are found on horizontal bonds (Fig. 2).

The point $J_2/J_1 = 1$ is special: there are $\mathcal{O}(2^L)$ degenerate ground states on an $L \times L$ lattice to order $1/S$. There is no Néel order even at zero temperature. Still, long-range bond order is present: if a single tetrahedron is put in the red state, there are no green tetrahedra on the same sublattice. By averaging over all red-and-blue states (Fig. 4) one obtains a magenta phase in which *antiparallel* spins, $\langle \mathbf{S}_i \cdot \mathbf{S}_j \rangle = -S^2$, are found on horizontal bonds. (For the rest of first and second neighbors,

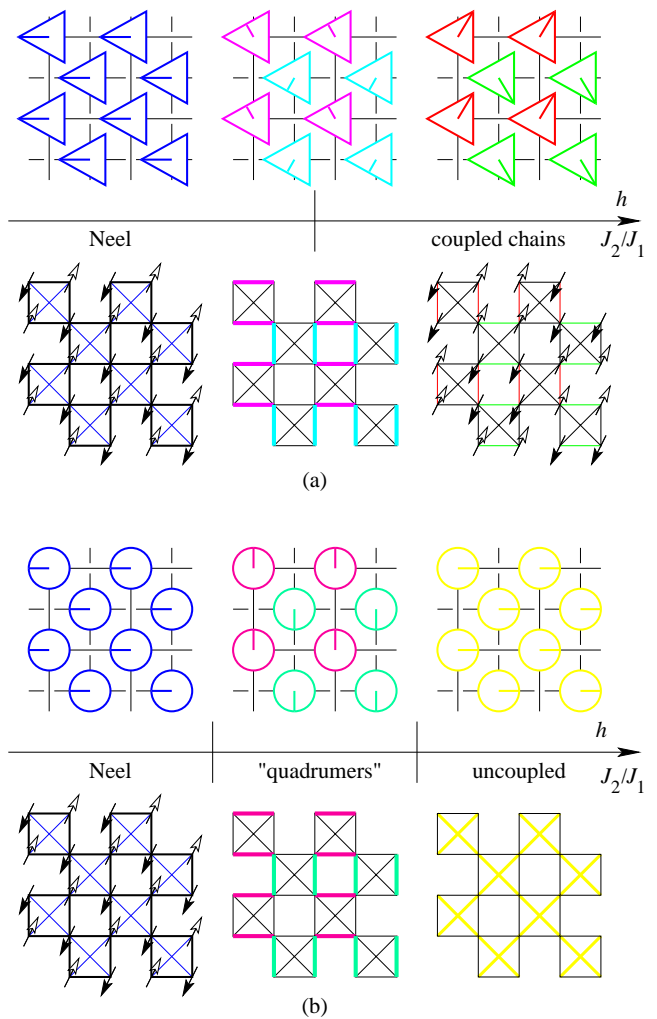


FIG. 6: (a) Ground states computed to order $1/S$ as a function of J_2/J_1 . The two sublattices of tetrahedra are colored independently of each other. (b) Ground states for $S = 1/2$ (Refs. 19,25,26,27). The secondary colors (cyan, magenta, and yellow) encode the location of satisfied bonds (those with antiparallel spins). They are the opposites of the primary-color states (respectively, red, green, and blue).

($\langle \mathbf{S}_i \cdot \mathbf{S}_j \rangle = 0$.) The cyan phase, where $\langle \mathbf{S}_i \cdot \mathbf{S}_j \rangle = -S^2$ on vertical bonds and 0 on the rest, is obtained by averaging over the green-and-blue states.

The independent ordering of the two sublattices of tetrahedra is probably accidental: the quantum correction of order $1/S$ (23) couples bond variables of the same sublattice. Higher-order corrections may well produce intersublattice couplings locking the sublattice order parameters.

As we have shown for $J_2/J_1 = 1$, parametrization of the four-spin interaction (24) in color terms gives a Potts-like model with $q = 3$ states and direction-dependent interactions (Fig. 5). Small deviations of the difference J_2/J_1 from 1 amount to adding a magnetic field h promoting or suppressing the blue state. For $J_2/J_1 < 1$ (blue field), it is advantageous to place *parallel* spins on

the weaker diagonal bonds making the entire lattice blue. For $J_2/J_1 > 1$, the field points in the opposite—yellow—direction suppressing the blue state and forcing the system to choose between the red and green states. Lastly, $J_2/J_1 = \infty$ is the regime of decoupled diagonal chains. The phase diagram is shown schematically in Fig. 6(a).

VI. QUANTUM LIMIT: $S = 1/2$

It is interesting to compare our large- S answers to the numerical results for $S = 1/2$ obtained recently.^{25,26,27} For $J_1 = J_2$ they have found a bond-ordered state in which the probability of finding a spin singlet is enhanced on half of the squares without crossings, the “quadramer” phase in Fig. 6(b). A similar plaquette state has appeared in the analyses of the quantum dimer model for the planar pyrochlore²³ and the Shastry-Sutherland lattice.⁴⁰ In our terminology, this plaquette state corresponds to the magenta-cyan vacuum [Fig. 6(a)]: the spin correlations $\langle \mathbf{S}_i \cdot \mathbf{S}_j \rangle$ are more negative on vertical bonds for one sublattice of tetrahedra and on horizontal bonds for the other. The $S = 1/2$ ground state quantum wavefunction, however, cannot be expressed as a simple product of single tetrahedron configurations.

Although the large- S and $S = 1/2$ answers are the same at equal couplings, there are also important differences that become apparent when we compare the results for $J_1 \neq J_2$. In the large- S phase diagram [Fig. 6(a)], the magenta-cyan state is a single point sandwiched between the blue and red-and-green phases. For $S = 1/2$, it is found in a finite range of ratios J_2/J_1 around 1. The phase diagram for $S = 1/2$ inferred from the works of Lhuillier *et al.* is shown in Fig. 6(b).

The $S = 1/2$ case does not lend itself to a straightforward analytical treatment. Nevertheless, we have found a useful phenomenological approach that sheds some light onto its phase diagram. The bond variables \mathbf{f} , which we have introduced previously for classical spins (20), can be defined in the same way for any spin value S . The ground states of an isolated tetrahedron with a Heisenberg interaction between its four spins are $2S + 1$ degenerate singlets. The operators $\hat{\mathbf{f}} = (\hat{f}_1, \hat{f}_2)$,

$$\begin{aligned} \hat{f}_1 &= \frac{(\mathbf{S}_1 + \mathbf{S}_2) \cdot (\mathbf{S}_3 + \mathbf{S}_4) - 2(\mathbf{S}_1 \cdot \mathbf{S}_2 + \mathbf{S}_3 \cdot \mathbf{S}_4)}{\sqrt{12}}, \\ \hat{f}_2 &= \frac{(\mathbf{S}_1 - \mathbf{S}_2) \cdot (\mathbf{S}_3 - \mathbf{S}_4)}{2}. \end{aligned} \quad (29)$$

leave this manifold of states invariant. In this Hilbert space they act as Hermitian matrices $(2S+1) \times (2S+1)$.⁴¹ In particular, for $S = 1/2$ they are proportional to the Pauli matrices. One can choose a basis in which

$$\hat{f}_1 = \frac{\sqrt{3}}{2} \tau_x, \quad \hat{f}_2 = \frac{\sqrt{3}}{2} \tau_z. \quad (30)$$

If the interaction between the bond variables on different tetrahedra α and β were of the pure Potts form, it

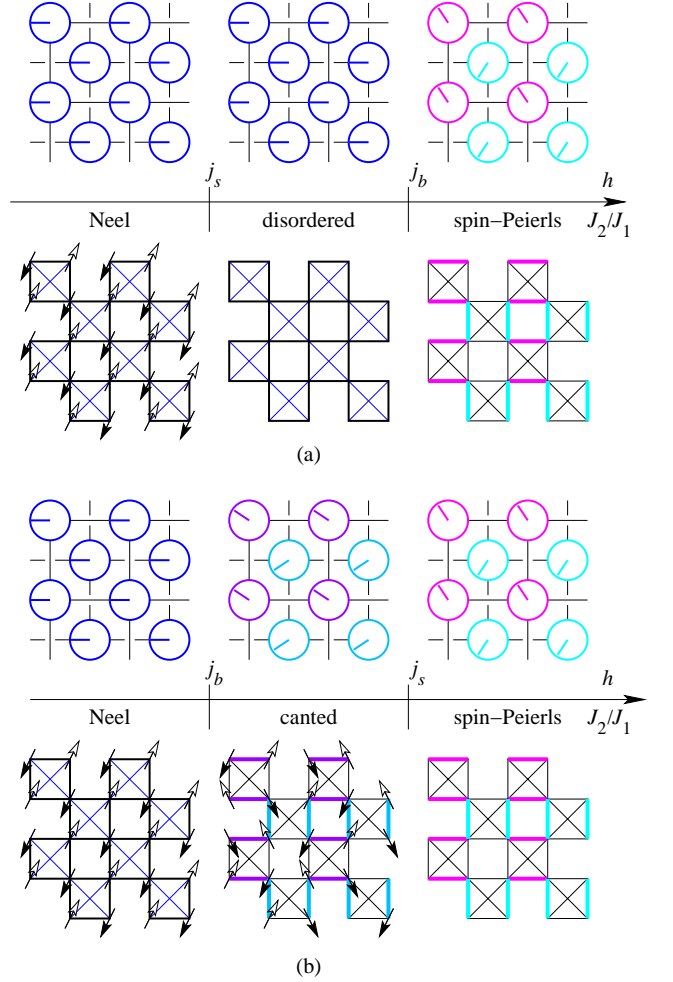


FIG. 7: Transitions between the Néel and “quadramer” states. (a) Spin order melts at $J_2/J_1 = j_s$, bond order appears at $J_2/J_1 = j_b > j_s$. (b) Spin order becomes noncollinear at $J_2/J_1 = j_b$, then disappears at $J_2/J_1 = j_s > j_b$.

would be proportional to the scalar product $\mathbf{f}_\alpha \cdot \mathbf{f}_\beta$. In the $S = 1/2$ case,

$$\mathbf{f}_\alpha \cdot \mathbf{f}_\beta = \frac{3}{4} (\tau_{\alpha x} \tau_{\beta x} + \tau_{\alpha z} \tau_{\beta z}). \quad (31)$$

However, as we have seen in Sec. IV C, the interaction has a more complicated form. It is direction-dependent and is asymmetric in the Potts flavors: red and green are different from the blue even when $J_1 = J_2$. The crudest way to reflect this asymmetry is to write an interaction of the form $K_1 f_{\alpha 1} f_{\beta 1} + K_2 f_{\alpha 2} f_{\beta 2}$ with $K_1 \neq K_2$. In addition, there can be a “magnetic field” coupling $-h f_{\alpha 1}$ that selects the blue states (for $J_2 \ll J_1$) or the red and green states ($J_2 \gg J_1$) in the classical case.

$$H = \sum_{\langle \alpha \beta \rangle} [K_{xx}(R_{\alpha\beta}) \tau_{\alpha x} \tau_{\beta x} + K_{zz}(R_{\alpha\beta}) \tau_{\alpha z} \tau_{\beta z}] - h \sum_{\alpha} \tau_{\alpha x}. \quad (32)$$

Here we assume for simplicity that the potentials K_{xx} and K_{zz} depend on the distance between tetrahedra, but

not on the direction. Our findings in the previous section indicate that the second-neighbor coupling is ferromagnetic ($K < 0$). Numerical results of the Fouet *et al.*²⁵ suggest that the nearest-neighbor interaction is antiferromagnetic ($K > 0$). The fact that the Ising order parameter is always related to the component f_2 points to the dominance of the K_{zz} coupling over K_{xx} . In this case we can neglect the K_{xx} terms altogether without changing the critical properties in any significant way:

$$H = \sum_{\langle\alpha\beta\rangle} K(R_{\alpha\beta})\tau_{\alpha z}\tau_{\beta z} - h \sum_{\alpha} \tau_{\alpha x}. \quad (33)$$

This is the Hamiltonian of an Ising antiferromagnet in a transverse magnetic field, whose properties are well known. At $h = 0$, it is a classical system with long-range order: $\langle\tau_z\rangle = +1$ on one sublattice and -1 on the other. (The tetrahedra form a square lattice, so that the interactions are not frustrated.) The Néel phase is preserved in a finite range of weak magnetic fields $|h| \lesssim K$. A strong “magnetic field” $h \gg K$ induces fast quantum fluctuations that kill the Néel order even at zero temperature, so that $\langle\tau_z\rangle = 0$. The zero-temperature phase diagram is shown in Fig. 6 (b). The system (33) has an “antiferromagnetic” phase for $|h| < h_c$, which corresponds to the “quadramer” state of Fouet *et al.*²⁵ Quantum critical points at $h = \pm h_c$ separate this phase from the quantum disordered regions with no bond order—the yellow and blue states in which the diagonal bonds are strong ($\langle\tau_x\rangle > 0$) and weak ($\langle\tau_x\rangle < 0$), respectively.

Let us pause for a moment and take a critical look at this phenomenology. From the viewpoint of bond variables, at some value $J_2/J_1 = j_c \approx 1$, which corresponds to $h = 0$, conditions are ideal for a spin-Peierls state: quantum fluctuations induced by the “transverse field” $h \propto J_2/J_1 - j_c$ are absent, so that bond order is robust. Going away from that point increases quantum fluctuations of $f_2 \propto \tau_z$ and reduces the bond order parameter until the bond order completely melts at a quantum critical point. If the critical behavior is adequately described by the Ising model, the energy gap vanishes at the critical point only. Both phases—bond-ordered and bond-disordered—are gapped.

This may or may not be the case. Consider in more detail the transition from the Néel phase of the simple square lattice ($J_2/J_1 = 0$) to the spin-Peierls phase at $J_2/J_1 \approx 1$. There are three distinct possibilities: (1) As J_2/J_1 increases, first the spin order melts at $J_2/J_1 = j_s$, then a bond order appears at $J_2/J_1 = j_b > j_s$, see Fig. 7 (a). The intermediate phase has neither spin, nor bond order. The critical behavior near $J_2/J_1 = j_b$ is adequately described by our bond phenomenology. (2) Magnetic order persists into the spin-Peierls phase. The spin and bond orders coexist⁴² in the range $j_b < J_2/J_1 < j_s$. In this case, the emergence of bond order at $J_2/J_1 = j_b$ is more adequately described as a spin canting transition, see Fig. 7 (b). The system is gapless on both sides of this quantum phase transition. (3) The spin order disappears simultaneously with the onset of the bond order

at $J_2/J_1 = j_s = j_b$, as shown in Fig. 6 (b). One phase is gapped, the other is gapless.

As is the usual limitation of exact diagonalisations, the numerical data of Sindzingre *et al.*²⁶ were obtainable only for moderately small lattices (up to 6×6). On the basis of their data we are unable to tell whether or not the spin and bond orders overlap. We feel, however, that all three possibilities can be realised as a matter of principle, so the Ising phenomenology may be useful.

VII. CONCLUSION

In this paper, we have studied the ground state of a Heisenberg antiferromagnet with large spins S on the checkerboard lattice, also known as the planar pyrochlore. To zeroth order in $1/S$ —the classical approximation—the magnet has an extremely large, continuous degeneracy of the ground state. In the next order in $1/S$, this accidental degeneracy is partially lifted by quantum fluctuations. The main achievement of this work is a complete characterization of the ground-state properties of this magnet to order $1/S$.

The ground states with the lowest energy of zero-point motion are found among the classical vacua with collinear spins. By using a special dynamical symmetry discovered by Henley,¹³ we have explicitly constructed all of these ground states and shown that their number is of order 2^L in a lattice $L \times L$. We have shown that there is no long-range Néel order: in the ensemble of these ground states spin correlations $\langle\mathbf{S}_i \cdot \mathbf{S}_j\rangle$ vanish beyond nearest neighbors. However, there is a long-range *bond* order: “tetrahedra” of the checkerboard lattice spontaneously pick up one of the two states, in which the nearest-neighbor correlations $\langle\mathbf{S}_i \cdot \mathbf{S}_j\rangle$ are uniformly $-S^2$ for vertical bonds and 0 for horizontal ones—or vice versa. The bond order breaks the rotational symmetry of the lattice.

More precisely, the bond order parameter is $\mathbf{Z}_2 \times \mathbf{Z}_2$: the two sublattices of tetrahedra order *independently* of each other, which is reminiscent of the Ashkin–Teller model. The discrete character of the broken symmetry indicates that the bond order will likely survive at low temperatures. The critical properties of the thermal transition between the bond-ordered and paramagnetic states remain an open question.

In addition to the bond order, there is a *nematic* long-range order: every spin points along a common direction $\hat{\mathbf{n}}$ or its opposite $-\hat{\mathbf{n}}$.

Our large- S analysis is in reasonable agreement with numerical results for the $S = 1/2$ planar pyrochlore antiferromagnet obtained by Fouet *et al.*²⁵ and Berg *et al.*²⁷ They find a bond-ordered ground state of *almost* the same kind as we do. The ordering of the two sublattices of tetrahedra is no longer independent: opposite patterns of the bond order are chosen. The ground state at $S = 1/2$ appears to be a doubly degenerate spin singlet. Numerical data suggest the presence of a spin gap, which seems to rule out the presence of spin order of the Néel

or nematic type. This brings up the question of stability of the nematic order that we have found at large S . A recent calculation of Canals,⁴³ based on the Dyson–Maleev approximation, indicates that collinear ground states are locally stable at large S but could become unstable below some critical value S_c . Although the Dyson–Maleev scheme is not a controlled approximation for small S , Canals’ scenario is consistent with the results reported here and in Refs. 25,26,27.

A lack of symmetry between the first and second-neighbor bonds compels one to study a more general system with unequal first and second-neighbor exchanges $J_1 \neq J_2$. For large S , the deviation of $j = J_2/J_1$ from the critical value $j_c = 1$ plays the role of a “magnetic field” in the 3-state Potts model. The 3 flavors correspond to the 3 collinear ground states of spins on a tetrahedron (modulo a global rotation of the spins). They can be labelled by the location of frustrated bonds: diagonal, vertical, or horizontal. The “magnetic field” $h \propto J_2/J_1 - 1$ prefers the “diagonal” state when $J_2 < J_1$, in which case the ground state is unique and the lattice symmetries are intact. When $J_2 > J_1$, the “vertical” and “horizontal” states are favored, which leads to a spontaneous breaking of the rotational symmetry of the lattice. Still, even at the critical point $J_2/J_1 = 1$ the symmetry between the three flavors is not restored: the diagonal bonds remain different from the horizontal and vertical ones, so that the symmetry is still \mathbf{Z}_2 , rather than \mathbf{S}_3 . Accordingly, the order parameter is of the Ising, rather than the 3-state Potts, model. Put another way, only one component of the Potts order parameter is used: that which is orthogonal to the direction of the “magnetic field” h .

At large S , Néel order is present on both sides of the critical point $J_2/J_1 = 1$, but not at the critical point itself. For $J_1 < J_2$ (diagonal chains with a weak frustrated coupling) the Néel order is induced by quantum fluctuations of spins. There are signs that, for a sufficiently weak interchain coupling, $J_1 < J_{1c} = \mathcal{O}(J_2\sqrt{S}e^{-S/2})$, the Néel order may be destroyed. The fate of the bond order is unknown, although chances are that it is less susceptible to long-wavelength spin fluctuations.

While it may be unreasonable to expect quantitative information about small spin values from a $1/S$ expansion, we were tempted to make some general statements about the observed behavior of the $S = 1/2$ system.^{25,26,27} It appears that there is some family resemblance and that the zero-temperature phase diagrams for large S [Fig. 6(a)] and for $S = 1/2$ [Fig. 6(b)] can be understood in similar terms, as far as bond order is concerned. We find it plausible that the bond operators (represented for $S = 1/2$ by 2×2 Pauli matrices) behave as spins of an Ising antiferromagnet in a transverse magnetic field. The Ising order parameter is an expectation value of τ_z ; the “magnetic field” h couples to τ_x . In zero transverse field, there is a bond order of the antiferro type, as observed by Fouet *et al.* A nonzero transverse field $h \propto J_2/J_1 - j_c$ induces quantum fluctuations of the “spins” τ_z . At some critical value of the “field” the bond

order melts and the ordered phase has a finite extent, in agreement with the numerical work of Sindzingre *et al.*²⁶

It is rather intriguing to find a valence-bond solid without Néel order in the limit of large S . This result is probably not unique to the planar pyrochlore and we intend to pursue this avenue further by studying other lattices. In particular, it would be interesting to solve a similar problem on the three-dimensional pyrochlore lattice and determine the resulting phase. In that case, the S_3 symmetry of the Potts states is intact and the outcome should be different. There are further open questions. Are there lattices that contain valence-bond *liquids* at large S ? What happens at intermediate values of S ? We look forward to finding out.

Acknowledgments

We thank C. L. Henley for sharing his unpublished results. We are grateful to C. L. Broholm, A.V. Chubukov, S. Sachdev and S. L. Sondhi for useful discussions, and to P. Sindzingre for a careful reading of the manuscript. We acknowledge hospitality of the Lorentz Centre of Leiden University where part of this work was done. Financial support was provided in part by the Alfred P. Sloan Foundation (A.G.A.), Research Corporation Award No. CC5491 (O.A.S.), and the NSF Grant No. DMR-9978074 (O.T.).

APPENDIX: ORDER FROM DISORDER IN THE CHAIN LIMIT

Here we derive the results presented in Sec. II.

1. Notation

The starting point $J_1 = 0$ corresponds to completely decoupled chains running along the diagonal directions $\hat{\xi}$ and $\hat{\eta}$. For technical reasons, we will consider chains with an Ising anisotropy:

$$H_0 = J_2 \sum_i \delta [S_i^x S_{i+1}^x + S_i^y S_{i+1}^y] + S_i^z S_{i+1}^z \quad (\text{A.1})$$

Introduction of the anisotropy ($0 \leq \delta < 1$) helps stabilize the collinear ground state of a single chain: at the Heisenberg point ($\delta = 1$) Néel order along the chain is destroyed by quantum fluctuations. At the technical level, this is caused by a divergent $1/S$ correction to the staggered moment for $\delta = 1$.⁴⁴ Then, strictly speaking, the initial assumption of the long-range Néel order on the chain breaks down. Therefore we compute the effects of the interchain coupling at $\delta < 1$ and then take the Heisenberg limit $\delta \rightarrow 1$. Unlike the staggered magnetization, the energy of zero-point motion (2) does not have an infrared divergence. This justifies approaching the

Heisenberg limit $\delta \rightarrow 1$ from below.⁴⁴ (Note, however, that the interchain coupling is always taken to be of the isotropic, Heisenberg kind.)

At the Ising point, $\delta = 0$, the system has an extensive degeneracy: there are 2^L ground states. We parametrize them by introducing a single Ising variable ± 1 for every chain. Then, for example, on the m th chain along $\hat{\xi}$ —whose spins have coordinates $\mathbf{r} = (n + 1/2, m)$ —we have $S_{\mathbf{r}}^z = (-1)^{n+1} s_m S$. We will use the Holstein-Primakoff transformation keeping the terms of orders $S, S^{1/2}$ and 1. For a spin with $S^z > 0$,

$$\begin{aligned} S^z &= S - a^\dagger a, \\ S^+ &= \sqrt{2S} \sqrt{1 - \frac{a^\dagger a}{2S}} a = \sqrt{2S} a + O\left(\frac{1}{\sqrt{S}}\right), \\ S^- &= \sqrt{2S} a^\dagger \sqrt{1 - \frac{a^\dagger a}{2S}} = \sqrt{2S} a^\dagger + O\left(\frac{1}{\sqrt{S}}\right). \end{aligned}$$

For spins with $S_z < 0$ we rotate the reference frame about the direction $\hat{\mathbf{x}}$ through π . Then for a spin located on the m -th chain running along $\hat{\xi}$ we obtain

$$\begin{pmatrix} S_{\mathbf{r}}^x \\ S_{\mathbf{r}}^y \\ S_{\mathbf{r}}^z \end{pmatrix} = \begin{pmatrix} 1 & 0 & 0 \\ 0 & (-1)^{n+1} s_m & 0 \\ 0 & 0 & (-1)^{n+1} s_m \end{pmatrix} \times \begin{pmatrix} \frac{\sqrt{2S}}{2} (a_{\mathbf{r}} + a_{\mathbf{r}}^\dagger) \\ \frac{\sqrt{2S}}{2i} (a_{\mathbf{r}} - a_{\mathbf{r}}^\dagger) \\ S - a_{\mathbf{r}}^\dagger a_{\mathbf{r}} \end{pmatrix}, \quad (\text{A.2})$$

where $\mathbf{r} = (n + 1/2, m)$.

The effective potential generated by quantum fluctuations is a function of L Néel vectors $\hat{\mathbf{n}}_m$. Invariance under global spin rotations implies certain restrictions on the form of that function. For instance, a pairwise potential coupling chains with staggered magnetizations $\hat{\mathbf{n}}_1$ and $\hat{\mathbf{n}}_2$ must be a function of the scalar product $\hat{\mathbf{n}}_1 \cdot \hat{\mathbf{n}}_2$. In addition, symmetry of the lattice requires—for chains running in perpendicular directions—that the coupling be invariant under $\hat{\mathbf{n}}_1 \mapsto -\hat{\mathbf{n}}_1$, so that it must depend on $(\hat{\mathbf{n}}_1 \cdot \hat{\mathbf{n}}_2)^2$. With this in mind, we will compute the lowest-order effect— $\mathcal{O}(J_1^2)$ —as a function of $L(L-1)/2$ angles between staggered magnetizations $\theta_{mn} = \arccos(\hat{\mathbf{n}}_m \cdot \hat{\mathbf{n}}_n)$. The pairwise nature of this potential allows us to tilt the spins uniformly on all η chains. It is convenient to choose $\hat{\mathbf{n}}_1$ as the z direction and let $\hat{\mathbf{n}}_2$ lie in the yz plane.

For potentials coupling more than two chains, one must consider a general orientation of the staggered magnetizations involved. However, because the leading term (4) already selects collinear states, in higher orders we will work with collinear configurations only.

Thus for the n th η chain—whose spins reside at $\mathbf{r} = (n, m + 1/2)$ —we perform an additional uniform rotation in the yz plane:

$$\begin{pmatrix} S_{\mathbf{r}}^x \\ S_{\mathbf{r}}^y \\ S_{\mathbf{r}}^z \end{pmatrix} = \begin{pmatrix} 1 & 0 & 0 \\ 0 & (-1)^{m+1} t_n \cos \theta & (-1)^{m+1} t_n \sin \theta \\ 0 & -(-1)^{m+1} t_n \sin \theta & (-1)^{m+1} t_n \cos \theta \end{pmatrix} \times$$

$$\times \begin{pmatrix} \frac{\sqrt{2S}}{2} (a_{\mathbf{r}} + a_{\mathbf{r}}^\dagger) \\ \frac{\sqrt{2S}}{2i} (a_{\mathbf{r}} - a_{\mathbf{r}}^\dagger) \\ S - a_{\mathbf{r}}^\dagger a_{\mathbf{r}} \end{pmatrix} \quad (\text{A.3})$$

Naturally, the intra-chain Hamiltonian is not affected by these unitary rotations:

$$H_0 = J_2 S \sum_{\mathbf{r}} \left[2a_{\mathbf{r}}^\dagger a_{\mathbf{r}} + \delta (a_{\mathbf{r}} a_{\mathbf{r}+\hat{\xi}} + a_{\mathbf{r}}^\dagger a_{\mathbf{r}+\hat{\xi}}^\dagger) \right] \quad (\text{A.4})$$

for the ξ chain. After a Fourier transform,

$$H_0 = J_2 S \sum_p \left[2a_p^\dagger a_p + \delta \cos p (a_p a_{-p} + a_p^\dagger a_{-p}^\dagger) \right], \quad (\text{A.5})$$

where p is the lattice momentum along the chain direction. Thermal Green's functions are given by

$$\langle a^\dagger(\omega, p) a(-\omega, -p) \rangle = \frac{\omega_0 - i\omega}{\omega^2 + \epsilon_p^2} \quad (\text{A.6})$$

$$\langle a(\omega, p) a(-\omega, -p) \rangle = -\frac{\omega_0 \gamma_p}{\omega^2 + \epsilon_p^2}, \quad (\text{A.7})$$

where ω is a bosonic Matsubara frequency and

$$\begin{aligned} \omega_0 &= 2J_2 S, \\ \gamma_p &= \delta \cos p, \\ \epsilon_p &= \omega_0 \sqrt{1 - \gamma_p^2}. \end{aligned} \quad (\text{A.8})$$

The perturbation term in the Hamiltonian (for which we introduce no anisotropy)

$$V = \sum_{n,m} J_1 (\mathbf{S}_{n-1/2,m} + \mathbf{S}_{n+1/2,m}) \cdot (\mathbf{S}_{n,m-1/2} + \mathbf{S}_{n,m+1/2}) \quad (\text{A.9})$$

ouples linear combinations of spins $\mathbf{S}_{n-1/2,m} + \mathbf{S}_{n+1/2,m}$ and $\mathbf{S}_{n,m-1/2} + \mathbf{S}_{n,m+1/2}$. Note that both linear combinations live on the same tetrahedron centered at (n, m) . It is convenient to introduce variables ξ_{nm} and η_{nm} representing transverse spin fluctuations on the respective diagonal links of the tetrahedron. For a link along $\hat{\xi}$,

$$\mathbf{S}_{n-\frac{1}{2},m} + \mathbf{S}_{n+\frac{1}{2},m} = 2\sqrt{S} \begin{pmatrix} \xi_{nm}^x \\ s_m (-1)^{n+1} \xi_{nm}^y \\ s_m (-1)^{n+1} \xi_{nm}^z \end{pmatrix}. \quad (\text{A.10})$$

By direct comparison to (A.2) we obtain

$$\begin{aligned} \xi_{nm}^x &= \frac{1}{2\sqrt{2}} (a_{n-\frac{1}{2},m}^\dagger + a_{n-\frac{1}{2},m} + a_{n+\frac{1}{2},m}^\dagger + a_{n+\frac{1}{2},m}), \\ \xi_{nm}^y &= \frac{i}{2\sqrt{2}} (a_{n-\frac{1}{2},m}^\dagger - a_{n-\frac{1}{2},m} - a_{n+\frac{1}{2},m}^\dagger + a_{n+\frac{1}{2},m}), \\ \xi_{nm}^z &= 0. \end{aligned} \quad (\text{A.11})$$

The longitudinal component ξ^z is of order $S^{-1/2}$ and has therefore been dropped at the current level of approximation. For η chains we similarly define η^a fields via

$$\begin{aligned} \eta_{nm}^x &= \frac{1}{2\sqrt{2}} (a_{n,m-\frac{1}{2}}^\dagger + a_{n,m-\frac{1}{2}} + a_{n,m+\frac{1}{2}}^\dagger + a_{n,m+\frac{1}{2}}), \\ \eta_{nm}^y &= \frac{i}{2\sqrt{2}} (a_{n,m-\frac{1}{2}}^\dagger - a_{n,m-\frac{1}{2}} - a_{n,m+\frac{1}{2}}^\dagger + a_{n,m+\frac{1}{2}}), \\ \eta_{nm}^z &= 0. \end{aligned} \quad (\text{A.12})$$

The sum of the spins along an η link is then expressed, according to (A.3), as

$$\mathbf{S}_{n,m-\frac{1}{2}} + \mathbf{S}_{n,m+\frac{1}{2}} = 2\sqrt{S} \begin{pmatrix} \eta_{nm}^x \\ (-1)^{m+1} t_n \cos \theta \eta_{nm}^y \\ (-1)^m t_n \sin \theta \eta_{nm}^y \end{pmatrix} \quad (\text{A.13})$$

The interchain coupling (A.9) now reads

$$V = 4J_1 S \sum_{n,m} (\xi_{nm}^x \eta_{nm}^x + \bar{\xi}_{nm}^y \bar{\eta}_{nm}^y), \quad (\text{A.14})$$

where we have introduced a shorthand notation

$$\bar{\xi}_{nm}^y = (-1)^n s_m \xi_{nm}^y, \quad \bar{\eta}_{nm}^y = (-1)^m t_n \cos \theta \eta_{nm}^y. \quad (\text{A.15})$$

To complete the preparation stage we work out Green's functions of the ξ and η variables for uncoupled chains:

$$\langle \xi_{nm}^a(\tau) \xi_{n'm'}^b(\tau') \rangle = \delta_{mm'} G^{ab}(\tau - \tau', n - n') \quad (\text{A.16})$$

$$\langle \eta_{nm}^a(\tau) \eta_{n'm'}^b(\tau') \rangle = \delta_{nn'} G^{ab}(\tau - \tau', m - m') \quad (\text{A.17})$$

where indices a and b take on values x and y . The space-time Green's functions $G^{ab}(\tau, n)$ are easily obtained in terms of their Fourier transforms,

$$G^{ab}(\tau, n) = \frac{1}{\beta} \sum_{\omega} \int_{-\pi}^{\pi} \frac{dp}{2\pi} G^{ab}(\omega, p) e^{-i\omega\tau + ipn} \quad (\text{A.18})$$

which are given by the matrix

$$\hat{G}(\omega, p) = \begin{pmatrix} \frac{\omega_0(1-\gamma_p) \cos^2(p/2)}{\omega^2 + \epsilon_p^2} & \frac{-i\omega \sin(p/2) \cos(p/2)}{\omega^2 + \epsilon_p^2} \\ \frac{-i\omega \sin(p/2) \cos(p/2)}{\omega^2 + \epsilon_p^2} & \frac{\omega_0(1+\gamma_p) \sin^2(p/2)}{\omega^2 + \epsilon_p^2} \end{pmatrix}. \quad (\text{A.19})$$

Partial Fourier transforms $G^{ab}(\omega, n)$ are real and satisfy the following identities:

$$\begin{aligned} G^{xx}(\omega, n) &= (-1)^n G^{yy}(\omega, n) = G^{xx}(\omega, -n), \\ G^{xy}(\omega, n) &= G^{yx}(\omega, n) = -G^{xy}(\omega, -n), \\ G^{xy}(\omega, n) &= (-1)^{n+1} G^{xy}(\omega, n). \end{aligned} \quad (\text{A.20})$$

The last line suggests that the off-diagonal components vanish for *even* distances n . At the Heisenberg point, the diagonal components vanish for *odd* distances.

2. Order J_1^2

The first nonvanishing correction to the free energy comes at the second order in J_1^2 and can be expressed as the second moment of the Euclidian action:

$$E^{(2)} = -\frac{1}{2!\beta} \left\langle \left(\int_0^\beta d\tau V \right)^2 \right\rangle. \quad (\text{A.21})$$

The perturbation V given by Eq. (A.14). Its second moment contains quartic averages

$$\langle (\xi_{nm}^x \eta_{nm}^x + \bar{\xi}_{nm}^y \bar{\eta}_{nm}^y) (\xi_{n'm'}^x \eta_{n'm'}^x + \bar{\xi}_{n'm'}^y \bar{\eta}_{n'm'}^y) \rangle. \quad (\text{A.22})$$

(Time variables are omitted for brevity.) Dependence on the staggered magnetizations s_m and t_n and the tilting

angle θ comes through the y components—see Eq. (A.15). Furthermore, terms containing two x and two y components vanish by symmetry: they have one factor of s only and staggered magnetizations s_m are odd under reflections in any line of spins along η . Therefore the only possibility is four y components:

$$\begin{aligned} \langle \bar{\xi}_{nm}^y \bar{\eta}_{nm}^y \bar{\xi}_{n'm'}^y \bar{\eta}_{n'm'}^y \rangle &= (-1)^{m+m'+n+n'} \cos^2 \theta \\ &\times s_m s_{m'} t_n t_{n'} \langle \xi_{nm}^y \xi_{n'm'}^y \rangle \langle \eta_{nm}^y \eta_{n'm'}^y \rangle, \end{aligned} \quad (\text{A.23})$$

where we have used Gaussian statistics of the variables ξ and η . It is evident that lattice points (nm) and $(n'm')$ must belong to a ξ chain and an η chain simultaneously, so that they are the same point. This term therefore gives rise to a contact interaction of crossing chains. The correction to the energy of a ground state is found by taking the limit of zero temperature ($\beta \rightarrow \infty$):

$$\begin{aligned} E^{(2)} &= -\frac{(4J_1 S)^2}{2!} \int \frac{d\omega}{2\pi} [G^{yy}(\omega, 0)]^2 \sum_{mn} \cos^2 \theta \\ &= -I(\delta) \frac{J_1^2 S}{J_2} \sum_{mn} (\hat{\mathbf{n}}_m \cdot \hat{\mathbf{n}}_n)^2, \end{aligned} \quad (\text{A.24})$$

where $\hat{\mathbf{n}}_m$ and $\hat{\mathbf{n}}_n$ are the directions of staggered magnetizations on chains running in the ξ and η directions, respectively; $G(\omega, 0)$ is the real-space Green's function $G(\omega, n)$ at distance $n = 0$. The numerical constant $I(\delta)$ is given here for the Ising ($\delta = 0$) and Heisenberg ($\delta = 1$) limits:

$$I(0) = \frac{1}{4}, \quad I(1) = \frac{4 - \pi}{2\pi}. \quad (\text{A.25})$$

Eq. (A.24) constitutes an order-by-disorder effect: collinear spin configurations ($\hat{\mathbf{n}}_m = \pm \hat{\mathbf{n}}_n$) minimize the energy of quantum fluctuations. There are 2^L such collinear states in an $L \times L$ lattice with periodic boundary conditions. Their degeneracy is partially lifted at the order J_1^4 , as we discuss next.

3. Order J_1^4

In the remainder of this section we will consider collinear vacua. Therefore the unitary transformation matrix in Eq. (A.3) becomes diagonal and (A.13) acquires the same form as (A.10). The ground-state energy will depend on the Ising variables s and t . The first non-trivial correction to the energy comes from the term of the fourth order in J_1 :

$$E^{(4)} = -\frac{1}{4!\beta} \left\langle \left(\int d\tau V \right)^4 \right\rangle. \quad (\text{A.26})$$

The dependence on staggered magnetizations s and t comes through the vertex $\xi^y \bar{\eta}^y$ (A.15). Symmetry arguments used in the preceding calculation show that s and t -dependent diagrams must contain exactly two vertices $\xi^x \eta^x$ and two $\xi^y \bar{\eta}^y$. We obtain

$$\begin{aligned}
E^{(4)} = & -2 \times 6 \times \frac{(4J_1 S)^4}{4! \beta} \int \frac{d\omega}{2\pi} \sum_{k,l,m,n} [(-1)^k s_m s_{m+k} G^{xy}(\omega, l) G^{yy}(\omega, k) G^{yx}(\omega, -l) G^{xx}(\omega, -k) \\
& + (-1)^l t_n t_{n+l} G^{xx}(\omega, l) G^{xy}(\omega, k) G^{yy}(\omega, -l) G^{yx}(\omega, -k) \\
& + (-1)^{l+k} s_m s_{m+k} t_n t_{n+l} G^{xy}(\omega, l) G^{yx}(\omega, k) G^{xy}(\omega, -l) G^{yx}(\omega, -k)]. \quad (\text{A.27})
\end{aligned}$$

Feynman diagrams contributing to Eq.(A.27) consist of a rectangular path formed by two ξ chains and two η chains (Fig. 8). The factors 2×6 have a combinatorial origin. At this order, the interchain coupling J_1 generates a two-chain interaction (between parallel chains) and a four-chain one (involving four crossing chains):

$$\begin{aligned}
E^{(4)} = & \frac{2J_1^4 S}{J_2^3} \sum_{l>0} \sum_{k>0} \sum_m \sum_n (A_k s_m s_{m+k} \quad (\text{A.28}) \\
& + A_l t_n t_{n+l} - B_{kl} s_m s_{m+k} t_n t_{n+l}),
\end{aligned}$$

Dimensionless couplings $A_l \geq 0$ and $B_{kl} \geq 0$ are

$$\begin{aligned}
A_k &= 2^7 (J_2 S)^3 \int \frac{d\omega}{2\pi} [G^{xx}(\omega, k)]^2 \sum_l [G^{xy}(\omega, l)]^2, \\
B_{kl} &= 2^8 (J_2 S)^3 \int \frac{d\omega}{2\pi} [G^{xy}(\omega, k)]^2 [G^{xy}(\omega, l)]^2. \quad (\text{A.29})
\end{aligned}$$

They fall off quickly with the distances k and l . We have used the properties of the Green's functions (A.20) in deriving them. Below we discuss the Ising ($\delta = 0$) and Heisenberg ($\delta \rightarrow 1$) limits.

a. Ising limit

In the Ising limit, the magnons ξ and η have an infinite mass and are unable to move far along the chain. Therefore $G^{ab}(\omega, l) = 0$ for $|l| > 1$. As a result, the effective potential depends on the nearest-neighbor products $s_m s_{m+1}$ and $t_m t_{m+1}$:

$$\begin{aligned}
E_{\text{Ising}}^{(4)} = & \frac{1}{128} \frac{J_1^4 S}{J_2^3} \sum_m \sum_n (s_m s_{m+1} + t_n t_{n+1} \\
& - s_m s_{m+1} t_n t_{n+1}). \quad (\text{A.30})
\end{aligned}$$

It is minimized by the ground states (9), in which staggered magnetizations have opposite signs on neighboring parallel chains. Such configurations minimize every term in Eq. (A.30).

b. Heisenberg limit

At the Heisenberg point, diagonal (off-diagonal) components of the propagator (A.19) contain even (odd) harmonics of the translation operator e^{ik} only. In real-space

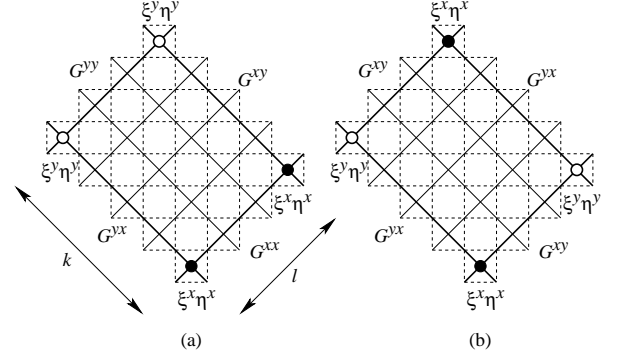


FIG. 8: Computation of the quantum correction to the free energy at $\mathcal{O}(J_1^4)$. Filled dots represent vertices $\xi_{mn}^x \eta_{mn}^x$, open ones $\xi_{mn}^y \eta_{mn}^y$; the latter contribute a factor $(-1)^{m+n} s_m t_n$ to the diagram. (a) The first term in Eq. (A.27). The diagram has a prefactor $(-1)^l t_n t_{n+l}$. (b) The third term in Eq. (A.27). Prefactor $(-1)^{k+l} s_m s_{m+k} t_n t_{n+l}$.

terms, a magnon can travel an even distance by keeping its polarization, an odd distance by flipping it. Thus pairwise chain interactions are induced for parallel chains with an even separation; quartic ones involve pairs of parallel chains with an odd separation:

$$\begin{aligned}
E^{(4)} = & \frac{2J_1^4 S}{J_2^3} \sum_{k=1}^{\infty} \sum_{l=1}^{\infty} \sum_m \sum_n (A_{2k} s_m s_{m+2k} \quad (\text{A.31}) \\
& + A_{2l} t_m t_{m+2l} - B_{2k-1, 2l-1} s_m s_{m+2k-1} t_n t_{n+2l-1}).
\end{aligned}$$

The dimensionless coefficients A and B are given below. As previously noted, this potential is invariant under a reversal of spins on every other diagonal chain (6). We will discuss the origin of this dynamical symmetry in Sec. III and demonstrate that it holds to an arbitrary order in J_1 .

The dominant term in (A.31)—proportional to $B_{1,1}$ —describes a coupling of four chains intersecting around an open square. It is minimized by spin configurations in which diagonal chains running in the same direction have either constant staggered magnetizations (8), or alternating ones (9). These states—shown in Fig. 2 (b) through (e)—are related by a staggering transformation (6). Therefore they remain degenerate even upon the inclusion of all two- and four-chain interactions in Eq. (A.31).

The second-largest term—a two-chain potential proportional to A_2 —is minimized by Néel states of a dif-

ferent kind: the ones with opposite staggered magnetizations for *second*-neighbor chains. Thus we obtain another viable candidate for a ground state:

$$s_{4n} = s_{4n+1} = -s_{4n+2} = -s_{4n+3} \quad (\text{A.32})$$

and similarly for t .

Because the fourth-order energy correction (5) contains oscillating terms, it is best to evaluate the energies at order J_1^4 exactly. We find that the energy of the states (8) and (9) is indeed lower by CJ_1^4S/J_2^3 per spin, where

$$C = \frac{\sqrt{2}}{4} - \frac{45}{128} \approx 1.991 \times 10^{-3}. \quad (\text{A.33})$$

4. Coupling coefficients A_l and B_{kl}

In what follows we specialize to the Heisenberg case, $\delta = 1$. Coefficients (A.29) of the two- and four-chains interaction (5) are given in terms of the following integrals

$$\begin{aligned} G^{xx}(\omega, n) &= \frac{\omega_0}{2} \int_{-\pi}^{\pi} \frac{dp}{2\pi} \frac{\sin^2 p e^{ipn}}{\omega^2 + \omega_0^2 \sin^2 p}, \\ G^{xy}(\omega, n) &= \frac{\omega}{2i} \int_{-\pi}^{\pi} \frac{dp}{2\pi} \frac{\sin p e^{ipn}}{\omega^2 + \omega_0^2 \sin^2 p}. \end{aligned} \quad (\text{A.34})$$

Introduce an auxiliary variable u :

$$\omega = \omega_0 \sinh u. \quad (\text{A.35})$$

We find:

$$G^{xx}(\omega, n) = \begin{cases} \frac{\delta_{n0} - \tanh |u|}{2\omega_0} e^{-|nu|} & n \text{ is even} \\ 0 & n \text{ is odd,} \end{cases} \quad (\text{A.36})$$

where δ_{mn} is the Kronecker delta;

$$G^{xy}(\omega, n) = \begin{cases} 0 & n \text{ is even,} \\ \frac{\tanh u}{2\omega_0} e^{-|nu|} \operatorname{sgn} n & n \text{ is odd.} \end{cases} \quad (\text{A.37})$$

$$\sum_n [G^{xy}(\omega, n)]^2 = \frac{\tanh |u|}{8\omega_0^2 \cosh^2 u}. \quad (\text{A.38})$$

Substituting these into Eq. (A.29) produces the following expressions for nonvanishing coupling constants in the

effective potential (A.28):

$$\begin{aligned} A_l &= \int_0^1 \frac{dx}{2\pi} \frac{(1-x)^3 x^{|l|-1/2}}{(1+x)^4}, \quad l \text{ is even,} \\ B_{kl} &= \int_0^1 \frac{dx}{2\pi} \frac{(1-x)^4 x^{|k|+|l|-3/2}}{(1+x)^3}, \quad k \text{ and } l \text{ are odd.} \end{aligned} \quad (\text{A.39})$$

Numerical values for the first few terms are:

$$\begin{aligned} A_2 &= 1.41 \times 10^{-3}, \quad B_{1,1} = 6.86 \times 10^{-3}, \\ A_4 &= 1.63 \times 10^{-4}, \quad B_{1,3} = 3.47 \times 10^{-4}, \\ A_6 &= 3.84 \times 10^{-5}, \quad B_{1,5} = B_{3,3} = 5.29 \times 10^{-5}. \end{aligned} \quad (\text{A.40})$$

Although these coupling constants fall off rather quickly—as $|l|^{-4}$ and $(|k| + |l|)^{-5}$ at large distances—partial cancellations in Eq. (A.28) call for a careful comparison of energies of the candidate ground states. In a state with equal staggered magnetizations on all chains (8), all products $s_m s_{m+k} = t_m t_{m+l} = 1$. The fourth-order correction to the energy is

$$\frac{E_{++++}^{(4)}}{N_{\text{spins}}} = \frac{J_1^4 S}{J_2^3} \left(2 \sum_{l=1}^{\infty} A_{2l} - \sum_{k=1}^{\infty} \sum_{l=1}^{\infty} B_{2k-1, 2l-1} \right) \quad (\text{A.41})$$

per spin. The state with alternating staggered magnetizations (9) is degenerate with it by virtue of the staggering symmetry (6). In the $(+- -)$ state (A.32), $s_m s_{m+k}$ oscillates as a function of m (and thus averages out to zero) for an odd k and equals $(-1)^{k/2}$ for an even k . Hence the expression for the correction to the ground-state energy at this order:

$$\frac{E_{+-+-}^{(4)}}{N_{\text{spins}}} = \frac{J_1^4 S}{J_2^3} \times 2 \sum_{l=1}^{\infty} A_{2l} (-1)^l. \quad (\text{A.42})$$

The energy difference is then

$$\frac{E_{+-+-}^{(4)} - E_{++++}^{(4)}}{N_{\text{spins}}} = C \frac{J_1^4 S}{J_2^3} > 0, \quad (\text{A.43})$$

where the constant is

$$\begin{aligned} C &= \int_0^1 \frac{dx}{2\pi} \frac{(1-x)^2 (1-4x+x^2) x^{1/2}}{(1+x)^5 (1+x^2)} \\ &= \frac{\sqrt{2}}{4} - \frac{45}{128} \approx 1.991 \times 10^{-3}. \end{aligned} \quad (\text{A.44})$$

* Electronic address: olegt@jhu.edu

† Electronic address: oleg.starykh@hofstra.edu

‡ Electronic address: moessner@lpt.ens.fr

§ Electronic address: alexandre.abanov@sunysb.edu

¹ G. H. Wannier, Phys. Rev. **79**, 357 (1950); R. M. F. Houtappel, Physica **16**, 425 (1950).

² P. Schiffer and A. P. Ramirez, Comments Cond. Mat. Phys.

18, 21 (1996).

³ M.J. Harris and M.P. Zinkin, Mod. Phys. Lett. B **10**, 417 (1996).

⁴ J.E. Greedan, J. Mater. Chem. **11**, 37 (2001).

⁵ J. Villain, Z. Phys. B **33**, 31 (1979).

⁶ A.B. Harris, A.J. Berlinsky, and C. Bruder, J. Appl. Phys. **69**, 5200 (1991).

- ⁷ N. Read and S. Sachdev, Phys. Rev. Lett. **66**, 1773 (1991).
- ⁸ P.W. Anderson, Science **235**, 1196 (1987).
- ⁹ S.-H. Lee *et al.*, Nature (London) **418**, 856, (2002); cond-mat/0208587.
- ¹⁰ Y. Yamashita and K. Ueda, Phys. Rev. Lett. **85**, 4960 (2000); cond-mat/0010504.
- ¹¹ O. Tchernyshyov, R. Moessner, and S.L. Sondhi, Phys. Rev. Lett. **88**, 067203 (2002); cond-mat/0108505.
- ¹² S.-H. Lee, C. Broholm, T.H. Kim, W. Ratcliff II, and S.-W. Cheong, Phys. Rev. Lett. **84**, 3718 (2000); cond-mat/9908433.
- ¹³ C.L. Henley (unpublished). We have presented the essential points of Henley's method in Sections III and IV C.
- ¹⁴ O. Tchernyshyov, R. Moessner, and S.L. Sondhi (unpublished).
- ¹⁵ A. Koga and N. Kawakami, Phys. Rev. B **63**, 144432 (2001); cond-mat/0010138.
- ¹⁶ H. Tsunetsugu, J. Phys. Soc. Japan **70**, 640 (2001); cond-mat/0103231.
- ¹⁷ H. Tsunetsugu, Phys. Rev. B **65**, 024415 (2002).
- ¹⁸ W. Brenig and A. Honecker, Phys. Rev. B **65**, 140407 (2002).
- ¹⁹ O.A. Starykh, R.R.P. Singh, and G.C. Levine, Phys. Rev. Lett. **88**, 167203 (2002); cond-mat/0106260.
- ²⁰ R. Liebmann, *Statistical mechanics of periodic frustrated Ising systems* (Springer, New York, 1986).
- ²¹ E.H. Lieb and P. Schupp, Phys. Rev. Lett. **83**, 5362 (1999); math-ph/9908019.
- ²² M. Elhajal, B. Canals, C. Lacroix, Can. J. Phys. **79**, 1353 (2001); cond-mat/0104331.
- ²³ R. Moessner, O. Tchernyshyov, and S.L. Sondhi, cond-mat/0106286.
- ²⁴ S.E. Palmer and J.T. Chalker, Phys. Rev. B **64**, 94412 (2001); cond-mat/0102447.
- ²⁵ J.-B. Fouet, M. Mambrini, P. Sindzingre, and C. Lhuillier, cond-mat/0108070.
- ²⁶ P. Sindzingre, J.-B. Fouet, and C. Lhuillier, Phys. Rev. B **66**, 174424 (2002); cond-mat/0204299.
- ²⁷ E. Berg, E. Altman, and A. Auerbach, Phys. Rev. Lett. **90**, 147204 (2003).
- ²⁸ T. Oguchi, Phys. Rev. **117**, 117 (1960).
- ²⁹ O. Tchernyshyov, cond-mat/0308091.
- ³⁰ R. Moessner and J.T. Chalker, Phys. Rev. Lett. **80**, 2929 (1998); cond-mat/9712063.
- ³¹ R. Moessner and J.T. Chalker, Phys. Rev. B **58**, 12049 (1998); cond-mat/9606177.
- ³² E.F. Shender, Sov. Phys. JETP **56**, 178 (1982).
- ³³ C.L. Henley, J. Appl. Phys. **61**, 3962 (1987).
- ³⁴ P. Chandra, P. Coleman, and A.I. Larkin, Phys. Rev. Lett. **64**, 88 (1990).
- ³⁵ See, e.g., T. Yildirim, A.B. Harris, and E.F. Shender, Phys. Rev. B **53**, 6455 (1996).
- ³⁶ A. Chubukov, Phys. Rev. B **44** 392 (1991).
- ³⁷ T. Yildirim, A.B. Harris, E.F. Shender, Phys. Rev. B **58**, 3144 (1998).
- ³⁸ O.A. Starykh (unpublished).
- ³⁹ P.M. Chaikin and T.C. Lubensky, *Principles of Condensed Matter Physics* (Cambridge University Press, New York, 1995).
- ⁴⁰ C.H. Chung, J.B. Marston, and S. Sachdev, Phys. Rev. B **64**, 134407 (2001); cond-mat/0102222.
- ⁴¹ O. Tchernyshyov, R. Moessner, and S.L. Sondhi, Phys. Rev. B **66**, 064403 (2002); cond-mat/0204154.
- ⁴² Coexistence of bond and spin orders has been considered previously by S. Sachdev and K. Park, Ann. Phys. (NY) **298**, 58 (2002); cond-mat/0108214.
- ⁴³ B. Canals, Phys. Rev. B **65**, 184408 (2002); cond-mat/0102233.
- ⁴⁴ I. Affleck, J. Phys.: Condens. Matter **1**, 3047 (1989).